Rift structure and sediment infill of hyperextended continental crust: Insights from 3D seismic and well data (Xisha Trough, South China Sea)

Chao Lei[1,2], Tiago M. Alves[3], Jianye Ren[1,2], Chuanxin Tong[4]

[1]Key laboratory of Tectonics and Petroleum Resources of Ministry of Education, China University of Geosciences, Wuhan 430074, China

[2]College of Marine Science and Technology, China University of Geosciences, Wuhan 430074, China

[3]3D Seismic Lab, School of Earth and Ocean Sciences, Cardiff University, Main Building, Park Place, Cardiff, CF10 3AT, United Kingdom

[4]China National Offshore Oil Corporation Ltd., Zhanjiang 524057, China

Corresponding authors: Chao Lei (clei@cug.edu.cn)； Jianye Ren (jyren@cug.edu.cn)

Key Points:

- The continental crust in the Xisha Trough was thinned by a detachment fault system;
- Post-rift units were moderately faulted within two distinct breakup sequences;
- Sediment influx changed from proximal to distal, and from transverse to axial, with progressive crustal extension

Abstract

Three-dimensional seismic and well data from the deepwater Xisha Trough are used to investigate the rift structure and sediment infill of a region formed adjacently to the initial oceanic ridge of the South China Sea (SCS). The high-quality data interpreted here permitted a detailed analysis of features such as: (1) detachment faults soling out at the Moho, (2) rotated and thinned continental blocks covered by thick sediment, and (3) changes in the location of basin depocenters resulting from detachment faulting. During the continental rifting phase (Eocene to earliest Oligocene), faulting was broadly distributed in Xisha Trough and resulted in the generation of isolated grabens/half-grabens filled by proximal sediment sources. During continental breakup in the Northwest Ocean Sector of SCS (early Oligocene to late Oligocene), extension became restricted to a narrow region where highly tilted continental blocks and thin crust were formed. Sediment was, at that time, fed to distal depocenters, which are presently bounded by listric faults rooted in a basal detachment. Later in a second stage (early Miocene), synchronously with continental breakup in the Southwest Ocean Sector of the SCS, the study area was blanketed by thick sediment. During the two continental breakup events, the hyperextended Xisha Trough was affected by closely spaced, small-scale faults rather than large basement-related structures. Our study highlights the effect of continental breakup as a way to broaden sediment influx from multiple sources into deepwater basins. As a corollary, this work recognizes two distinct *breakup sequences* in the Xisha Trough, and concludes on their geodynamic significance to the South China Sea.

1 Introduction

Studies of rifted continental margins across the world have, in the past, benefited from seismic and borehole data from deepwater regions offshore Iberia [*Boillot et al., 1987; Sawyer et al., 1994; Tucholke and Sibuet, 2007; Whitmarsh et al., 1997*], where complex tilted block geometries are observed in continental slope basins [*Manatschal, 2004; Alves et al., 2009; Reston et al., 2009*]. Seismic and borehole data from rifted continental margins such as the Bay of Biscay [e.g. *Tugend, 2014*], West Africa [e.g. *Unternehr et al., 2010*], Norwegian Sea [e.g. *Gernigon et al., 2012; Peron-Pinvidic and Osmundsen, 2016*], East India [e.g. *Nemčok et al., 2013*], the conjugate South Australian and Antarctica margins [e.g. *Gillard et al., 2015*], as well as from outcropping fragments of the Mesozoic Tethys Ocean [e.g. *Manatschal, 2004; Masini et al., 2012; Mohn et al., 2012; Tugend et al., 2014*], reveal comparable first-order crustal architectures to West Iberia, with crustal thickness decreasing from the continental shelf toward deepwater basins. In particular, the region closest to the oceanic crust, comprising hyperextended crust, shows an average thickness below 10 km [e.g. *Peron-Pinvidic et al., 2013*].

Great part of the existing tectono-stratigraphic models for rifted margins are focused on their proximal domains [e.g. *Allen and Allen, 2013*], although great progress has been recently made on some of the most studied distal margins [*Alves et al., 2006; 2009; Autin et al., 2010; Decarlis et al., 2015; Haupert et al., 2016; Lei et al., 2019a; Masini et al., 2012 and 2013; Pereira and Alves, 2012; Soares et al., 2012; Bai et al., 2019; Ding et al., 2019*]. In these latter regions, seismic data reveal structural styles and depositional patterns that are markedly complex [e.g. *Lymer et al., 2019; Larsen et al. 2018; Lei et al. 2019a; Lizaralde et al. 2007; Gillard et al., 2015; Ding et al., 2019*], including fault geometries that cannot be fully explained by the classical rift models of *McKenzie* [1978] and *Wernicke* [1985]. In other published examples of distal domains (e.g., Bay of Biscay), most syn-rift structures are buried under younger foreland basins, hindering the complete characterization of their early stages of continental rifting [*Tugend et al.*, 2014]. Against such a background, to characterize and understand the stratigraphic architectures, depositional environments and sediment sources of sedimentary basins formed over hyperextended crust is still a major challenge to industry and academia.

The Xisha Trough, also named the eastern part of the Qiongdongnan Basin in the published literature [*Lei and Ren, 2016*], is located in the Northwest South China Sea between the Hainan Island-Shenhu Rise and the Xisha Islands (Figure 1a). Large scale, southeast- and south-dipping faults bound this trough to form an asymmetric structure at present (Figure 1b). The Xisha Trough formed ahead of a propagating oceanic ridge [*Briais et al., 1993; Sibuet et al., 2016; Cameselle et al., 2015*]; its continental lithosphere was deformed by the stretching and thinning processes that created the Northwest Ocean Sector of the South China Sea (SCS), but crust failed to break up at the exact location of the trough [*Lei and Ren, 2016*]. Therefore, the Xisha Trough comprises an example of how key structures and depositional processes evolve on extremely thinned, hyperextended continental crust prior to the propagation of continental breakup, which occurred from the earliest Oligocene to the Burdigalian (early Miocene) along the SCS (Figure 2).

The thickness and architecture of the Xisha Trough were previously investigated by 2D seismic profiles revealing hyperextended crust <10 km thick in its axis [*Qiu et al., 2001; Lei and Ren, 2016*]. This area of thinned crust, located in the eastern part of the Xisha Trough, is overlain by more than 10 km of syn- and post-

rift sediments [*Zhao et al., 2015*] and is located just westward of oceanic crust of the Northwest Ocean Sector of the SCS (Figures 1a and 1b). However, over the past decade, newly acquired 3D seismic surveys tied to stratigraphic data from Exploration Well CC1162 have been acquired in the Xisha Trough to investigate the rifting history of this region. One of these 3D seismic surveys covers the Changchang Subbasin of the Xisha Trough and its corresponding shoulder regions (Figure 1a and 1b). Exploration Well CC1162 drilled through sediments in the Changchang Subbasin, recovering strata as old as the lower Oligocene Yacheng Formation (Figure 3). By using these novel, high-quality 3D seismic and borehole data, this study aims to: 1) document the geometries of detachment faults, their overlying syn-rift sediments, and underlying basement in the Xisha Trough; 2) document the structural evolution of (early) post-rift strata comprising *breakup sequences* cf. *Soares et al.* [2012]; and 3) recognize major shifts in sedimentation patterns, along the Xisha Trough axis, in the context of the progressive continental breakup of the SCS. This study focuses on a specific example of a rift basin on the distal margin that has experienced hyperextension but failed to record full crustal breakup.

2 Geological Framework

The SCS is a marginal sea located in the western Pacific region and is a magma-intermediate passive margin classified between the 'classical' magma-poor and magma-rich types [*Larsen et al., 2018*]. It records a half-rate in ocean spreading of around 2.5 cm/yr after continental breakup was achieved [*Briais et al., 1993; Li et al., 2014*]. This rate is comparable with what *Searle* [2013] classified as an *intermediate seafloor spreading rate*. The SCS comprises a northern continental margin, an oceanic basin and a southern continental margin (Figure 2). The oceanic basin *per se* can be divided into distinct East, Northwest and Southwest Ocean Sectors, or Subbasins cf. *Briais et al.* [1993] (Figure 2).

The SCS resulted from continental rifting and breakup of the margin of the South China block [*Briais et al., 1993*] (Figure 2). Prior to the opening of the SCS, a wide area of extended crust was generated on the South China block and accumulated (syn-rift) sediments from surrounding sources [*Hall, 2012*]. *Franke et al.* [2014] have previously recognized a westward and later southward shift in continental breakup as the SCS opened, with *Zhao et al.* [2016a] later proposing that Late Cenozoic magmatism in the Baiyun Subbasin occurred during the deposition of distinct breakup stratigraphic sequences. In fact, IODP Expeditions 349, 367 and 368 estimate that seafloor spreading in the SCS started in the Eastern Ocean Sector at ~34-32 Ma (earliest Oligocene), ending in the East and Southwest Ocean Sectors at ~15 Ma and 16 Ma, respectively [*Briais et al., 1993*; *Li et al., 2014; Larsen et al., 2018*] (Figure 2). During this period, ocean-ridge spreading firstly stopped in the Northwest Ocean Sector at ~26 Ma, and then jumped to the Southwest Ocean Sector at ~23 Ma [*Briais et al., 1993*]. This oceanic ridge jump was also recorded on oceanic crust in the form of lower crust reflections dipping in opposite directions, ridgeward and landward [*Ding et al., 2018*]. Borehole data from the transition between oceanic and continental crust demonstrates that MORB-type basalt intruded underlying basement rocks, or was extruded in places, during these continental breakup events [*Larsen et al., 2018; Sun et al., 2018; Ding et al., 2019*].

At a regional scale, hyperextended crust has been previously imaged on seismic data along the Nam Con Son Basin [*Li et al., 2014; Savva et al., 2013*], offshore Southwest Taiwan [*McIntosh et al., 2014*], on the Southern margin of the SCS [*Savva et al., 2014*], in the Liwan Subbasin [*Lei et al., 2019*], in the Baiyun Subbasin [*Gao et al., 2015*] and in the Xisha Trough [*Lei and Ren, 2016*]. The Xisha Trough

comprises a V-shaped structure in map view, with extended crust continuing westward towards Indochina (Figure 2). The northern shoulder of the Xisha Trough thus coincides with the modern continental shelf, while its southern shoulder is located at the Xisha islands (Figure 1b). Main sedimentary depocenters in the Xisha Trough consist of the Songnan, Baodao and Changchang Subbasins (Figure 1b).

At present, the bathymetry of the Xisha Trough increases from approximately 900 m in the Songnan Subbasin to nearly 3200 m in the transitional domain between the Changchang Subbasin and the oceanic crust of the Northwest Ocean Sector (Figure 1b). Along the Xisha Trough, a 570 km long and 3-11 km wide canyon (Central Canyon), strikes from East to West (Figure 1a). This canyon is, at present, an important routing system for sediment reaching the oceanic basin [*Chen et al.*, 2015; *Su et al.*, 2019].

The study area is a 150 km-long, 70 km-wide asymmetric sedimentary rift (Changchang Subbasin) that strikes roughly E-W [*Zhao et al., 2015; Lei and Ren, 2016*] (Figure 1). The Changchang Subbasin is bounded by the Shenhu Rise to the Northeast, the Xisha Islands to the South, and by a flexure at the tip of the Xisha Trough to the NE (Figure 1b). The boundary between the western part of the Changchang Subbasin and the Baodao Subbasin coincides with a large magmatic edifice [*Lei and Ren, 2016*] (Figure 1b), while the eastern border of the Changchang Subbasin is close to the boundary between continental and oceanic crust.

The basement around the Changchang Subbasin, and the Xisha Trough as a whole, consists of metamorphic and igneous rocks from which samples have been recovered by exploration drilling. These rocks were formed at 140 Ma and 415 Ma based on U-Pb dating from detrital zircons [*Cui et al.*, 2018; *Zhu et al.*, 2017]. The Changchang Subbasin is also characterized by its relatively high heat flow, ranging from 85 to 105 mw/m^2 [*Shi et al.*, 2017]. Several km-scale magma edifices are observed in the center of the Xisha Trough, especially in and around the Changchang Subbasin [*Gao et al.*, 2019].

The crust in the Changchang Subbasin was thinned by multiple phases of extension and depth-dependent thinning [*Zhao et al., 2018a; Lei and Ren, 2016*]. As a result, key tectonic phases recorded in the Changchang Subbasin include: (1) widespread deformation that evolved, from the Paleocene to the Oligocene [*Zhao et al.*, 2015], from diffuse and widespread rifting to more localized crustal thinning [*Lei and Ren*, 2016]; (2) subsequent thermal cooling and post-rift subsidence in the Neogene [*Zhao et al., 2018b*; *Lei and Ren, 2016*]. Consequently, a recognized period of fast subsidence has prevailed in deepwater regions of the Xisha Trough since the end of continental breakup in the Southwest Ocean Sector of the SCS, at ~15 Ma [*Zhao et al.*, 2018b; *Xie et al.*, 2006]. This tectonic subsidence has been associated with lower crustal flow processes across the northern margin of the SCS [e.g. *Bai et al.*, 2019].

3. Data and Methods

3.1 3D seismic data

The Changchang Subbasin are mapped and analyzed in this work using a high-resolution 3D seismic survey (CVX3D; see Figures 1b and 1c) acquired in 2013 by Chevron and China National Offshore Oil Corporation (CNOOC). The interpreted seismic volume covers ~3000 km^2 of the central Changchang Subbasin at a water depth greater than 1 km (Figure 1b). The seismic volume was processed with a Common Mid-Point (CMP) spacing of 12.5 m, a main frequency bandwidth of ~30-45 HZ, and a recording length of 10.2 s two-way travel time (TWT). Seismic interpretation, as well as subsequent wireline-log analyses, were performed on Schlumberger's GeoFrame® software (Version 4.4). Seismic profiles were

interpreted every km so as to map the geometry of distinct fault systems, and to analyze their relationship with adjacent sedimentary units. Seismic coherence maps were compared with the interpreted volume and used to characterize the geometry of fault systems. The coherence technique is based on a comparison of waveforms across adjacent traces, and highlights discontinuous features such as faults and chaotic intervals against continuous background strata [*Hart, 1999; Marfurt and Alves, 2015*].

3.2 Borehole data

The seismic-stratigraphic framework established by *Lei et al.* [2016] was revised in this paper after considering the new sediment core data, gamma-ray and sonic logs acquired by Exploration Well CC1162 (water depth: 2154.35 m) in the Changchang Subbasin (Figures 1a and 1b). Well CC1162 was drilled in 2012 and reaches a depth of ~2056 meters below the seafloor. It drilled through 1016 m of Neogene and 1040 m of Paleogene strata (Figure 3).

The new stratigraphic framework proposed in this work subdivides the Cenozoic succession of the Xisha Trough into eight seismic-stratigraphic units: the Shixing, Yacheng, Lingshui, Sanya, Meishan, Huangliu, Yinggehai and Ledong Formations (Figure 3). These stratigraphic formations are separated by nine distinct seismic-stratigraphic markers: Tg, T80, T70, T60, T50, T40, T30, T20 and T0, representing major sequence boundaries across the Xisha Trough (Figure 3). The ages of the seismic units considered in this work are also constrained by biostratigraphic data from exploration wells in the Xisha Trough and its shoulder areas [*Xie et al., 2015*] (Figure 1a). Horizons Tg to T0 will be used as reference seismic-stratigraphic markers throughout this paper so as to define continental rifting, continental breakup and post-oceanic spreading sequences in great detail (Figure 3).

3.3 Detrital zircon U-Pb dating

Detrital zircon samples from rocks cored in the central part of the Xisha Trough were analyzed at the State Key Laboratory of Geological Processes and Mineral Resources, China University of Geosciences in Wuhan. Absolute ages based on $^{238}U/^{206}Pb$ for grains younger than 1 Ga and $^{207}Pb/^{206}Pb$ for grains older than 1 Ga were obtained for more than 93 zircons collected from the well-core samples [*Compston et al., 1992*]. The spectrum of grain-cooling ages from the samples is displayed in this work using the Kernel Density Estimation (KDE) method of *Vermeesch* [2013], which plots detrital ages as a set of Gaussian distributions, but does not explicitly take into account the analytical uncertainties of this method.

4. Seismic stratigraphy

4.1 Borehole-seismic correlation

Strata deposited on hyperextended crust of the Xisha Trough were sampled by Well CC1162 (Figure 1). Depositional facies were interpreted for the entire Cenozoic succession based on data from sediment and sidewall cores. Sidewall cores were acquired every 80 m in Miocene strata and every 10 m in Oligocene units. Wireline-log responses were calibrated with core descriptions, and helped to qualitatively interpret the main lithologies and depositional facies in uncored intervals (Figures 3 and 4). Wireline-log responses for Well CC1162 could only be calibrated for Oligocene-lower Miocene strata due to poor core recovery below and above these intervals.

The oldest stratigraphic unit in the study area, the Shixing Formation, was deposited above Horizon Tg (Figures 3, 5 and 6). The Shixing Formation is imaged as a high-amplitude homogenous package in Figure 6, and is bounded by a basement fault in the northeastern part of the study area (Figures 3, 5

and 6). The deepest lower Oligocene strata drilled by Well CC1162 belongs to the Yacheng Formation, comprising marine dark gray mudstones typical of littoral environments (Figures 3 and 4). On wireline data, littoral facies in the Yacheng Formation correlate with serrate gamma-ray curves and show low gamma-ray values (Figure 3). Seismic reflections in the Yacheng Formation are of low amplitude and good continuity (Figures 3, 5 and 6).

Overlying the Yacheng Formation is the upper Oligocene Lingshui Formation, which was cored in Well CC1162 to retrieve gray claystone interbedded with fine-grained, well sorted sandstones (Figures 3 and 4). These interbedded sandstones and mudstones are characterized by their relatively wide range (90-200 API) in gamma-ray values (Figure 3). Internal seismic reflections in the lower Lingshui Formation have low amplitude but good continuity, and comprise interbedded claystone and silts. In contrast, the upper Lingshui Formation consists of siltstones and fine sandstones imaged as strong amplitude, continuous seismic reflections (Figures 3, 5 and 6). The lower Sanya Formation overlies the Lingshui Formation to contain gray claystone interbedded with gray carbonate debris (Figure 3 and 4). The lower Sanya Formation is ~460 m thick, characterized by a funnel-shaped gamma-ray curve and a blocky density-log signature (Figure 3). The upper Sanya Formation shows variable density values (2.0-3.0 g cm^{-3}) and comprises gray claystone interbedded with thin layers of siltstone (Figure 3). The upper Sanya Formation comprises a 350 m thick clay succession with gamma-ray values between 140 and 80 API (Figures 3). Overlying the Sanya Formation is the Meishan, Huangliu, Yinggehai and Ledong Formations, which were not cored by Well CC1162. Their internal seismic reflections show variable amplitude and good continuity (Figures 3, 5 and 6).

4.2 Seismic-stratigraphic framework

A key outcome of this work is the subdivision of Cenozoic strata in the Changchang Subbasin into nine regional seismic units (Figure 3). This new framework is based on the internal seismic character of imaged stratigraphic intervals, complemented by stratigraphic data from Well CC1162 and other exploration wells shown in Figures 1a and 1b.

Figure 5 shows a deep-penetration regional (2D) seismic profile across the Changchang Subbasin and its shoulder areas. In the Changchang Subbasin there is a rotated crustal block (Block A) and a relatively deep depression filled by thick sediment (Figure 5). Horizon Tg is a regional angular unconformity separating the pre-rift basement from syn-rift strata (Figure 5). Horizon Tg is locally offset by basement faults, especially those bounding discrete depocenters and accommodating heaves of several kilometers (Figure 5).

Horizon T80 is recognized as the first high-amplitude feature above Tg and separates the Shixing Formation from the Yacheng Formation (Figure 5). Internal reflections in strata deposited below Horizon T80 are generally chaotic in the shoulder areas of the Changchang Subbasin, but continuous in its central part, making the Shixing Formation hard to define in this region. Nevertheless, the Shixing Formation is characterized by a wedge-shaped architecture and was sampled by Exploration Well Y211 to reveal a thick succession of mudstones. Previous studies indicate that the Shixing Formation was deposited in a lacustrine setting [*Hao et al., 2000; Wang et al., 2014*].

Horizon T70 forms the boundary between rotated tilt-blocks with syn-rift sediment growing onto normal faults, and a more ‘passive’ interval covering the syn-rift topography and adjacent structural highs (Figures 3 and 5). Above T70, Horizon T60 comprises another distinct unconformity across

the study area. Near the shoulders of the Changchang Subbasin, Horizon T60 is an angular unconformity, but in the central part of the subbasin the horizon is relatively flat and concordant with older strata (Figure 5). On the seismic profile in Figure 6, it is also clear that basement faults did not propagate through Horizon T60; instead, some younger faults offset this same seismic stratigraphic marker to show very moderate displacements.

Strata delimited by Horizons T60 and T0 are not offset by basement faults and can be divided into five discrete seismic-stratigraphic packages (Figures 5 and 6). Horizon T50, a high amplitude reflector, marks the top of the Sanya Formation, which thins towards the northern shoulder of the Changchang Subbasin (Figure 6). In parallel, Horizons T40, T30 and T0 delimit conformable, moderate-amplitude strata in the study area. The exception to this rule is the southwest part of the profile in Figure 6, where internal reflections between Horizons T40, T30 and T0 are discontinuous due to the incision of a 10 km-wide submarine canyon (Central Canyon) in strata above T50. Above Horizon T30, chaotic and transparent seismic intervals are observed to the Northeast of the Central canyon and likely comprise mass-transport deposits (Figure 6).

Figure 7 shows two-way time (TWT) structure maps for the horizons interpreted on seismic data. Horizon Tg (top basement) shows relatively high relief ranging from 7000 ms to 8000 ms TWT. Basement highs are observed on the northern part of the 3D seismic volume, whereas relative lows are located in the center of the Changchang Subbasin (Figure 7a). Between successive depocenters, there are three structural highs at the level of Horizon Tg. The three structural highs reflect the presence of distinct crustal blocks, named herein as Blocks A, B and C (Figure 7a).

Although there are local variations in the depth and structure of the interpreted horizons, some common features are apparently unchanged through time. For instance, a relative low is observed throughout the Cenozoic in the central part of the Changchang Subbasin (Figure 7a-7i). Here, a prominent ESE-trending depocenter is observed at the level of Horizons T40 and T30 in Figures 7f and 7g, marking the presence of a submarine channel incising to a depth of 4200 ms TWT (Figures 5 and 6). The present-day structure (Figure 7i) of the central part of the Changchang Subbasin is dominated by a structural high to the West and a basin low to the East, a similar setting to that recorded at Horizon T50 and in younger strata, e.g. at the level of Horizons T40, T30, T20 and T0. The TWT structure maps for these different horizons reveal progressive smoothing of the inherited rift-related topography through time (Figures 7a-7i).

5. Mapping of hyperextended crust and associated faults

Seismic profile CC301 in Figure 8 images the regional structure of the Changchang Subbasin. In the shallower parts of the subbasin, the seismic reflector marking the base of the Cenozoic succession is a regional erosional surface draped and onlapped by Eocene strata. On this same seismic profile, Horizon Tg shows high-amplitude but is also discontinuous and offset by basement faults, e.g., Faults F18, F20, F21 and F22 (Figure 9). Horizon Tg separates the pre-rift basement with a homogeneous (crystalline) character from syn-rift strata above.

Underlying Horizon Tg is the acoustic basement, which is offset by normal faults showing throws of 1.2 s to 0.1 s TWT. Among the basement structures are four large-scale normal faults, F18, F20, F21 and F22, offsetting Paleogene strata and soling out at basement level (Figure 8). At the center of the seismic profile in Figure 8, Faults F20, F21 and F22 generate a step-down geometry from the Northern shoulder of the Xisha Trough towards the main depocenter. This step-down geometry is due to the presence three main structural highs, Blocks A, B and C, as highlighted on the

isochron map of Horizon Tg (Figure 7a). Within the basement, the Moho is characterized by its high-amplitude, continuous seismic reflections observed at ~9 s TWT in Figure 8. The volume of rock constrained by Horizon Tg and the Moho is interpreted to be continental crust.

Compared to the map of the Moho published in *Bai et al.* [2015], our high-quality 3D seismic data permits the identification of subtle variations in the depth of the Moho reflections (Figures 6 and 8). Continental crust in the central Changchang Subbasin was markedly extended, thinned, and is estimated to be only 0.9 s TWT thick, i.e. approximately 2.8 km thick considering a p-wave (Vp) velocity of 6.2 km/s for continental crust [*Xia et al., 2010*]. In comparison, the continental block bounded by Faults F22 and F21 is covered by strata at least 5.4 s TWT (7.1 km) thick (Figure 8). Continuous high-amplitude reflections are interpreted to be the Moho reflectors below continental crust, revealing a character similar to the Liwan Subbasin [*Larsen et al., 2018; Sun et al., 2018; Lei et al., 2019a*]. These high-amplitude reflections occur at a depth of ~9 s TWT throughout the study area, and are relatively continuous on the seismic profile in Figures 8. They are also observed on the NE-striking seismic profile in Figure 6, which is parallel to the 2D seismic profile in Figure 5.

It is worth stressing that several other reflections are identified within continental crust; these typically present abrupt lateral terminations and complex geometries (e.g. seismic reflections indicated by the arrows in Figure 6). These seismic features with high amplitude contrast remarkably with the surrounding crust, which shows diffractive, low-amplitude seismic reflections. We interpret these high-amplitude features as magmatic intrusions similar to structures observed underlying thick strata offshore central Norway [*Abdelmalak et al., 2017*]. Saucer-shaped structures are also observed in Figure 8, but at a depth of ~8 s TWT these strong reflectors become parallel to the Moho and become hard to map. The size of these intrusions is in the range of tens of kilometers.

In the Changchang Subbasin, continental crust and overlying sediment were intersected by normal faults with variable sizes. Faults F18, F20, F21, F22 deforming the Shixing, Yacheng and Lingshui Formations show variable offsets. Subsequent deformation of the Yacheng and Lingshui Formations was localized in the central Xisha Trough, where relatively larger offsets are observed in Faults F20, F21 and F22 when compared to Fault F18 (Figure 8). Strata above Horizon T60 were not offset by basement faults, being instead deformed by minor, closely-spaced faults (Figures 6 and 8; 3D seismic data). To the South, these small faults offset Horizon T60 and link with basement faults (Figures 6 and 8). Most of these minor normal faults terminate below Horizon T50, though a few also offset shallower strata deformed by slope instability (Figure 5). In addition, the small faults that offset strata below Horizon T50 in Figures 5 and 6 did not propagate into the basement.

Figure 9 shows coherence slices at 5000 ms TWT that image the deeper strata in the Changchang Subbasin. Faults shown on the coherence data are ESE-striking and mostly linear, although some parts of Fault F20 curve toward the NE in the center of the basin (Figure 9). To the north of Fault F20, the coherence slice intersects the crystalline basement to image only a few faults as relatively small structures offsetting Paleogene strata, at most (Figures 5 and 6). The central Changchang Subbasin is bounded by Faults F21 and F22, which are more than 40 km long in map view (Figure 9). The area between Faults F21 and F22 shows multiple small-scale faults, most of which are NE-striking in map view (Figure 9). These are related to the dense, small-offset faults in strata delimited by Horizons T60 and T50 (Figures 5, 6 and 8). Fault F18 was not well imaged on the coherence slice in Figure 9 due to poor coherence similarity across Fault F18 at

the level of 5000 ms TWT. However, this same Fault F18 is clearly observed on the vertical seismic profiles in Figures 5, 6 and 8. It is important to stress that Figure 9 images structures at a depth of 5000 ms TWT, meaning that faults formed in different tectonic events were mapped together. Fault orientations and their evolution will be addressed in the following section.

6. Sediment thickness across the distal domain of the Changchang Subbasin

6.1 Strata deposited during continental rifting: Eocene to lower Oligocene

Figure 10 shows a series of isopach maps for key stratigraphic units in the Changchang Subbasin. The thickness of strata deposited during continental rifting was variable due to the effect of the larger faults imaged in the coherence slice at 5000 ms TWT (Figures 9 and 10a). Relatively thin strata are observed in the northern part of the volume, where they are directly deposited above structural highs (Figures 5 and 6). The general trend of this thin interval of strata is East-West (Figure 10a). Between structural highs, strata can be 1400 ms thick in the central Changchang Subbasin, with minor depocenters dispersed across the basin.

Syn-rift strata can be divided into two formations, i.e. the Shixing and Yacheng Formations (Figures 10b and 10c). The Shixing Formation comprises strata deposited between the basement and Horizon T80, marking the development of multiple small depocenters bounded by ENE-striking faults (Figure 10b). Between Horizons T80 and T70 (Yacheng Formation) sediment is more widespread, bar a few ESE-trending depocentres bounded by relative large normal faults, e.g. Fault F20 (Figure 10c). The variable sediment thickness in syn-rift strata marks important fault activity during this period (Figures 10d-10i).

6.2 Strata deposited during continental breakup and oceanic spreading processes: upper Oligocene to lower Miocene

The interval between Horizon T70 and T50 reveals the thickest sediment in the central Changchang Subbasin, where up to 1500 ms TWT of strata are identified and mapped (Figures 10d and 10e). This interval is characterized by the little control syn-rift topography (and structures) had on sedimentation, with broad ESE-trending depocenters prevailing in the study area. Such a configuration was controlled by the ESE-striking Faults F20, F21 and F22, which developed by the growth and linkage of the same faults that controlled the thickness of the Yacheng Formation (earliest Oligocene). Other faults distant from the central Xisha Trough, i.e. Faults F18 and F23, became less important structures controlling sedimentation.

The Sanya Formation comprises the youngest strata in the Changchang Subbasin associated with continental breakup (Figures 3 and 10e). This formation shows a similar distribution to the oldest Breakup Sequence A (Lingshui Formation), with thinner strata occurring on the northern and southern shoulders of the Changchang Subbasin (Figures 3 and 10d). Depocenters appear to extend beyond our study area and reveal a relative thickening of sediment to the west (Figures 10d and 10e). Faults propagating from the basement were almost inactive at this time; instead, deformation by small faults predominated within a stage of widespread subsidence in the Xisha Trough (Figures 6 and 8). Such a pattern is also observed in the overlying drift-related Meishan and Huangliu Formations, although these intervals were incised by an ESE-striking Central Canyon (Figures 10f and 10g).

6.3 Post-Oceanic spreading interval: Middle Miocene to Holocene

Above Horizon T50, the distribution of strata in the Changchang Subbasin reveals a pattern that is very similar to the present day's (Figure 10f to 10i). The thickest sediment is observed in the central part of the Changchang Subbasin, while its shoulder areas show relatively thin strata. The central Subbasin strikes E-W and shows its largest thickness of sediment to the west (Figures 10f to 10h).

A submarine canyon crossing the Yinggehai Formation is observed on the isopach map in Figure 10h, where it reaches maximum thickness (300 ms TWT) in an ESE-striking direction. In contrast, the shoulders of the Changchang Subbasin record very little deposition during the time interval in which canyon incision occurred (2.6-5.5 Ma) (Figure 10h).

The Quaternary Ledong Formation presents a different geometry to the underlying units due to widespread slope instability and sediment bypass from the North and South into the Changchang Subbasin (Figures 5 and 10i).

7. U-Pb ages from detrital zircons

It is important to note that Exploration Well CC1162 is located in the study area (see Figure 1a), which is the closest to oceanic crust in the Northwest Ocean Sector of the SCS. It provides direct information about source-to-sink processes during continental rifting and breakup. Together with published U-Pb ages from location within and around the Xisha Trough [*Yan et al., 20111; Shao et al., 2016; Lei et al., 2019b*], this works analyzes 93 new U-Pb zircon ages for upper Oligocene sediments drilled by Well CC1162 (sample CC1162-1; Supplementary Table S1). Sediment grains from upper Oligocene strata show variable uranium concentrations (>47.1 ppm, and up to 2545.2 ppm), and highly variable Th/U ratios (0.51–131.84; see Supplementary Table S1). Upper Oligocene strata from Well CC1162 present similar age peaks to those in Exploration Well Y211 (sample Y211-1; Figure 11). These strata record major age peaks at 145 Ma, 240 Ma, and 420 Ma. However, the minor age peaks recorded at 915 Ma and 1810 Ma in Well Y211 are not prominent in the upper Oligocene samples from Well CC1162.

Zircon U-Pb ages for upper Oligocene samples acquired in the shoulder areas of the Xisha Trough cluster at the Yanshanian and Indosinian events (Figure 11). Their age distribution shows simple patterns, e.g., a single age peak for samples B611-1, YLSH and YC19-1; twin age peaks for QLSH and Y19-1. We stress that upper Oligocene strata are derived from the northern and southern shoulders of the Xisha Trough and, as a result, Wells CC1162 and Y211 show complex age distributions for such strata. In contrast, lower Oligocene strata show zircon U-Pb distribution patterns that are relative simple and cluster at 240 Ma, e.g., samples Y211-2 (Central Xisha Trough) and Y19-2 (southern shoulder of the Xisha Trough) (Figure 11).

Potential sediment provenance trends derived from U-Pb age spectra are shown in Figure 12. We analyzed 27 samples from potential sediment sources (Supplementary Table S2) to subdivide them into three types: 1) rivers and hinterland areas surrounding the Xisha Trough (Figure 12a) *[Yao et al., 2011; Xia et al., 2012; Sun et al., 2009; Xu et al., 2008; Cao et al., 2018; Clift et al., 2006; Hoang et al., 2009; Shao et al., 2017a; Jonell et al., 2017; Wang et al., 2018*], 2) basement rocks in the Xisha Trough and its corresponding shoulder areas (Figure 12b) [*Zhu et al., 2017; Cui et al., 2018; Xu et al.,2014; Cao et al., 2015; Wang et al., 2015*], and 3) Eocene and Oligocene sediments from the Pearl River Mouth Basin (Figure 12c) [*Shao et al., 2017b, 2019*]. Magma addition in the basement of the Xisha Trough has been recorded by Exploration Wells XK1 [*Zhu et al.*, 2017], B2 and B3 [*Cui*

et al., 2018]. Their zircon U-Pb ages cluster at 100 Ma, 140 Ma, 145 Ma, 240 Ma and 415 Ma, i.e., revealing a narrow spectrum of ages (Figure 12b). Sediment derived from the Hainan Island, part of the northern shoulder of the Xisha Trough, also has a narrow age spectrum with age peaks at 100 Ma and 240 Ma, similarly to basement rocks drilled by the Exploration Wells XK1, B2 and B3 mentioned above (Figure 12b).

8. Discussion

8.1 Sedimentation patterns ahead of a propagating oceanic ridge

Continental rifting, initiated in the Late Cretaceous-early Paleogene [*Taylor and Hayes, 1983; Holloway, 1982*], resulted in continental breakup and unequivocal generation of oceanic crust between the Late Oligocene and early Miocene in the SCS [*Larsen et al., 2018; Li et al., 2014*]. In the Changchang Subbasin we recognize that continental rifting occurred, at least, since the Eocene, as suggested by the presence of pre-Oligocene sediments controlled by basement faults. Lower Oligocene sediments were drilled by Well Y211, whose detrital zircons show an abundance of grains younger than 500 Ma, although with a common minority population that is older than 500 Ma (Figure 11). This characteristic is similar to strata deposited on the northern shoulder of Xisha Trough (samples YLSH and QLSH) [*Yan et al., 2011*], but is different to the age peak patterns of coeval sediments in the Pearl River Mouth Basin (Figure 12c).

Rivers and continental blocks around the Xisha Trough are likely to have been the main source of sediment to the study area, as indicated in Figure 12a, among which the Red and Pearl Rivers record the largest catchments. Except for the small-scale Song Tu River, the age patterns for sediment fed by rivers and hinterland sources show complex age peaks associated with Yanshanian, Indosinian, Kwangsian, Jinningian and Luliangian events. In the Pearl River Mouth Basin, the U-Pb age spectra for Eocene sediments are simple and narrow, with age peaks clustering at 115 Ma (U1435), or 115 Ma and 225 Ma (L21). Oligocene sediment in the Pearl River Mouth Basin has a wide zircon U-Pb age spectrum and age peaks are relatively more complex when compared to Eocene sediment. This contradicts the interpretation of a broad lower Oligocene sediment provenance from the Pearl River Mouth Basin to the Xisha Trough. However, our data does not entirely clarify if upper Oligocene sediment derived from the Pearl River Mouth Basin reached the Xisha Trough when considering the age peaks shown in Figures 11 and 12. This important detail can only be tested by multi-dimensional scaling (MDS) plots, in which similar samples are shown close together, while less similar samples are plotted farther apart [*Vermeesch, 2013*].

Figure 13 shows precisely one of such MDS plots to highlight the relative similarity of U-Pb ages between strata deposited in the Xisha Trough and potential sediment sources surrounding the study area. Upper Oligocene samples from Wells Y211 and CC1162 plot close together to show great affinity with sediment derived from modern river systems, e.g., the Red and Song Gianh Rivers (Figure 13). Such a sediment dispersion pattern suggests that upper Oligocene sediment was sourced from distal areas along the axis of the Xisha Trough. However, upper Oligocene sediment on the shoulders of the Xisha Trough appears not to be related to a more central, axial transport (Figure 13). Considering their U-Pb age peaks, we suggest that sediment deposited on the shoulders of the Xisha Trough was derived from proximal sources such as structural highs and other fault-bounded topography [e.g *Alves and Cupkovic, 2018*].

After the latest early Oligocene (~28.1 Ma), the main depocenter of the Xisha Trough migrated into the central Changchang Subbasin

in response to detachment faulting, although minor depocenters were formed earlier (Late Eocene) along the central Changchang Subbasin (Figures 10c-10h and 14). However, faulting on the shoulders of the Xisha Trough decreased in magnitude and importance after this time [*Lei and Ren, 2016*]. The basement of the central part of the Xisha Trough subsided relatively quickly and became a main depocenter, forming the main sediment route from the Red River to the Changchang Subbasin.

Below upper Oligocene sediment are strata whose U-Pb age patterns are simple and similar to strata deposited on the shoulders of the Xisha Trough (Figures 11 and 12). Lower Oligocene samples plot close to samples YLSH, QLSH and Y19-1, reflecting a sedimentation pattern controlled by continental rifting [*Yan et al., 2011*], filling the grabens and half-grabens imaged in seismic data [*Lei et al., 2016; Zhao et al., 2018b*]. Therefore, sedimentation was restricted at this time to local syn-rift depocenters, a very similar setting to the present-day Basin and Range province in North America [*Lei et al., 2016; Franke et al., 2014; Wernicke, 1981*]. When analyzed together with the isopach maps in Figures 10a to 10c, provenance trends further highlight that Eocene sediment filled isolated depocenters bounded by propagating faults (Figure 10b); subsequent lower Oligocene depocenters migrated to the east of our study area in response to active detachment faulting (Figure 10c). During both the Eocene and early Oligocene, sediment derived from the Red River was not transported into the Xisha Trough in large volumes due to the control syn-rift topography had on sedimentation, restricting most deposition to isolated (and relatively proximal) grabens and half-grabens.

In summary, the U-Pb age spectrum for the lower Oligocene strata presents simple and narrow age peaks, similar to that of surrounding highs within the basin. Eocene and early Oligocene depocenters bounded by basement faults were fed by sediment derived from proximal sources. Subsequent upper Oligocene sediment on the shoulders of the Xisha Trough was still derived from proximal sources. In contrast, upper Oligocene sediment along the central part of the Xisha Trough was mostly delivered from distal sources. In fact, the detrital zircon U-Pb data shows an affinity between sediment deposited in the central part of the Xisha Trough and sediment derived from the Red River. This study thus provides evidence for a fast shift in Oligocene sedimentary sources, from proximal to distal, at the transitional domain between continental and oceanic crust.

8.2 Hyperextended crust and its progressive evolution

During the Eocene and earliest Oligocene (Shixing and basal Yacheng Formations), a series of grabens and half-grabens bounded by high-angle normal faults were generated throughout the northern SCS [*Franke, 2014; Lei and Ren, 2016*]. During the Eocene, sediment filled small grabens and half-grabens, evenly distributed across the basin (Stage 1 in Figure 14). Rift-related structures did not significantly deform the crust and very little extension was accommodated by them [*Zhao et al., 2018b*]. The crust was not particularly thinned at this moment, and was likely similar to the thickness of present-day crust on the shoulders of the Xisha Trough (~25 km). This observation is consistent with faults propagating throughout the brittle upper crust [*Lei and Ren, 2016*] and with the limited amount of tectonic subsidence observed in graben/half-grabens of the Northern SCS at this time [*Zhao et al., 2015 and 2018b*]. As a result, the study area records the accumulation of sediment derived from proximal sources (Stage 1 in Figure 14).

Subsequent deformation was progressively focused in deepwater regions, especially as detachment faults were formed

along the transitional domain between thinned continental crust and oceanic crust, e.g., in the Tainan Basin [*McIntosh et al., 2014; Yeh et al., 2012*], the Jinghai-Xingning Subbasin [*Lei et al., 2018*], and the Liwan Subbasin [*Lei, et al., 2018*]. In these basins, most of the basement faulting terminated after ~33 Ma when continental breakup first occurred in the Eastern Ocean Sector of the SCS. In the Changchang Subbasin, the initiation of a detachment fault system comprising the larger Faults F20, F21 and F22 (Figures 5, 6 and 8), started at this precise moment (Stage 2 in Figure 14). These ESE-striking faults offset the crust and sole out at a basal decollement.

After this event, upper Oligocene-middle Miocene strata were mostly offset by small-scale faults, although basement faults continued to affect upper Oligocene strata, but recording minor offsets (Figures 6 and 8). Importantly, oceanic accretion in the SCS did not continue into our study area; instead ocean-ridge spreading migrated into the Southwest Ocean Sector of the SCS.

Previous numeric and analogue modeling argued that major depocenters are formed orthogonally to weak zones (e.g. pre-rift structures) during crustal extension, and that minor depocenters are generated along oblique weak zones (e.g. Corti et al., 2007). However, the 3D seismic data and 2D regional seismic profile in our study do not image any pre-rift structures, suggesting that continental rifting in the Xisha Trough was initiated on homogeneous crust. The extension direction during the Eocene and early Oligocene is predicted to be roughly N-S trending. Subsequent continental rifting during the deposition of the Yacheng and Lingshui Formations (Oligocene) denotes a change to a NNW to NW orientation of crustal extension (Figure 10b-10d). This denotes a slight clockwise rotation relative to the extension regime recorded during the Eocene.

An important observation from seismic data is that Horizon T70 separates seismic stratigraphic units with distinct geometries. Strata underlying Horizon T70 are wedged-shaped and grow markedly towards basin-bounding faults (Figures 5, 6 and 8), while the interval bounded by Horizons T70 and T60 is more widespread, covers adjacent structural highs, and is thicker at the center of half-graben and grabens (Figures 5, 6 and 8). Strata geometries across Horizon T70, i.e. intervals bounded by Horizons T70 and T60, and Horizons T70 and T80, indicate that Fault F18, and other minor faults on the tilt-blocks, nearly ceased to move before the late Oligocene (Figures 5, 6 and 8). Absolute ages in zircon grains from upper Oligocene samples vary from 32.9 to 3543 Ma, with dominant peaks at 145, 240, 430, 915 Ma that correspond to the Yanshanian, Indosinian, Kwangsian and Jinningian orogenic events, respectively (Figure 11). Compared to the underlying lower Oligocene Yacheng Formation, with a unique U-Pb age peak, sediment above Horizon T70 records age peaks that reflect multiple sediment sources around the Xisha Trough.

Another important unconformity in the study area is Horizon T60, which corresponds to a sediment hiatus aged ~24-28 on the marginal high (site U1501) [*Jian et al., 2019*]. In the central part the Xisha Trough this stratigraphic boundary correlates with a conformable surface due to continuous basement subsidence. Horizon T60 is a high-amplitude continuous seismic reflector separating underlying faulted sediment from relatively uniform strata above.

Sedimentation on the northern margin of the SCS, including the depositional hiatus at IODP Site U1501 and continuous high-amplitude strata in the Xisha Trough, indicate a ~23.8 Ma (uppermost Oligocene) age for the first event of oceanic crust formation to the south the Changchang Subbasin, e.g. in the Southwest Ocean Sector of the SCS. In fact, Briais et al. [1993] and *Barckhausen et al.* [2014] interpreted the onset of seafloor spreading in the Northwest and Southwest

Sectors of the SCS at ~33-30 Ma and ~23 Ma, respectively. This occurred together with a spreading-ridge jump from the Northwest to the Southwest Sectors at ~23 Ma.

In such a context, Horizon T60 marks the ~23 Ma episode of oceanic-ridge jump and onset of oceanic spreading in the Southwest Ocean Sector of the SCS. In contrast, the breakup unconformities at ODP Site 1148 in the Xingning-Jinghai Subbasin indicate continental breakup has initiated in this area at ~28-30 Ma based on nannofossil data [*Wang et al., 2000*]. Just to the south of ODP Site 1148, in the Eastern Ocean Sector of the SCS, the breakup unconformity is dated at ~33 Ma and separates poorly sorted sandstones from thin mudstones [*Li et al., 2014*]. After the cessation of oceanic spreading in the Northwest Ocean Sector of the SCS, and subsequent onset of oceanic spreading in the Southwest Ocean Sector at 23 Ma [*Briais et al.,1993; Li et al., 2014; Barckhausen et al., 2014*], the Changchang Subbasin was blanketed by strata bounded by T60 and T50 (Figure 14). In the interpreted seismic volume, minor faulting is still observed within this early Miocene interval (Figures 6 and 8). Overlying Horizon T50 are parallel strata showing no obvious growth onto faults.

Lithospheric breakup is a complex process, recording mantle breakup prior to or after crust breakup [*Huismans and Beaumont, 2011*], and progressive oceanic ridge propagation along continental margins [*Franke et al., 2014*]. Instead of a breakup unconformity responding to relatively simple, instantaneous breakup of continental crust [*Falvey, 1974; Braun and Beaumont, 1989*], recent work considered the lithosphere breakup event as being associated with a sedimentary sequence above, named a *breakup sequence* by *Soares et al.* [2012]. The breakup sequence was described as reflecting the period that spans from the onset of continental breakup to the establishment of thermal relaxation as the main process controlling regional subsidence. Based on the data in this paper and the known continental breakup events recorded in the SCS, we define two *breakup sequences* developing above Horizon T70 in association with prolonged (if moderate) faulting in the Changchang Subbasin. Breakup Sequence A spans the interval between Horizons T70 and T60 and relates to continental breakup in the Northwest Ocean Sector, i.e., just East of the study area (Figures 3 and 14). Moderate basement-fault activity is recorded at this time, with tilt-block rotation and accommodation-space creation clearly imaged below Horizon T70 (Figures 5, 6 and 14). Breakup Sequence B is associated with continental breakup in the Southwest Ocean Sector, and the top of this sequence can be defined by Horizon T50, dated at 16 Ma [latest Burdigalian; see *Zhao et al., 2016*] (Figures 3, 6, 8 and 14). Such an interpretation follows the concepts in *Alves et al.* [2009] and *Alves and Cunha* [2018] for West Iberia, in which *breakup sequences* (and the unconformities that bound them) become successively younger as continental breakup propagates along a continental margin. In the study area, these *breakup sequences* become younger southwestwards, reflecting the gradual propagation of continental breakup from East to West along the northern SCS [*Franke et al., 2014; Zhao et al., 2016; Cameselle et al., 2015*]. Stacked breakup sequences are expected to accumulate in the regions that were synchronously rifted at first, during the early stages of continental rifting, but record progressive, diachronous continental breakup (Figure 14).

9. Conclusions

During the Cenozoic, the Xisha Trough was located at the tip of an E-W rift axis in the northern SCS, whose structure and sedimentation patterns document the transient stage preceding the change from continental rifting towards a fully rifted margin. In this study, 3D seismic and well data best illustrate the fault systems affecting different

stratigraphic levels in the Changchang Subbasin, including basal decollements and ancillary normal faults. It also gives important insights on the multiple sources of sediment that fed the Changchang Subbasin. The main results in this work can be summarized as follows:

(a) During the initial stages of continental rifting, sedimentation was controlled by high angle faults, and isopach maps show that faults were broadly distributed in the study area.

(b) Progressive crustal stretching and faulting was expressed in the form of large detachment faults formed between the Late Eocene and Early Oligocene. At the end of this stage, in the Early Oligocene, continental breakup was initiated in its Eastern Ocean Sector.

(c) Continental breakup in the Northwest Sector, just to the eastern side of our study area, resulted in the generation of a first Breakup Sequence A. This sequence records the migration of the main basin depocenter toward the central part of the Changchang Subbasin. Depocenters were filled with sediment transported axially to the Xisha Trough. Sediment delivery from the Red River started in the late Oligocene, as shown by detrital zircon U-Pb data.

(d) Early Miocene faulting continued in the study area, at a time when the Southwest Ocean Sector of the SCS recorded continental breakup. We propose that early Miocene faulting resulted from plate readjustments associated with the onset of oceanic accretion in the Southwest Ocean Sector of the SCS. These faults occur within a younger Breakup Sequence B.

Acknowledgments

We thank two anonymous reviewers for their detailed comments and suggestions, which help to substantially improve the manuscript. Grants from Natural Science Foundation of China (No. 41772093; 41830537), State Oceanic Administration of China (GASI-GEOGE-02), National Key Research and Development Project (2017YFC1405502), and National Science and Technology Major Project of the Ministry of Science and Technology of China (2016ZX005008-001-001) are acknowledged. We are grateful to the CNOOC for providing access to the seismic data and for permission to publish this paper. The reflection seismic profiles and detrital zircon U-Pb data used in this study are available at https://pan.baidu.com/s/18SzneuLCxuzZ1UD-uXLIxw by entering the extraction code “gen2”.

References

Abdelmalak, M. M., et al. (2017), The T-Reflection and the Deep Crustal Structure of the Vøring Margin, Offshore mid-Norway, *TECTONICS*(36), 2497-2523.

Allen, P.A. and J.R. Allen, Basin analysis: Principles and application to petroleum play assessment. 2013: John Wiley & Sons.

Alves, T. M., et al. (2006). Mesozoic–Cenozoic evolution of North Atlantic continental-slope basins: The Peniche basin, western Iberian margin. *AAPG Bull., 90*, 31-60. doi: 10.1306/08110504138

Alves, T. M., and T. Cunha (2018), A phase of transient subsidence, sediment bypass and deposition of regressive–transgressive cycles during the breakup of Iberia and Newfoundland, 596 *EARTH PLANET SC LETT*, *484*, 168-183.

Alves, T. M., et al. (2009), Diachronous evolution of Late Jurassic-Cretaceous continental rifting in the northeast Atlantic (west Iberian margin), *TECTONICS*, *28*(TC4003), 1-32.

Autin, J., et al. (2010), Continental break-up history of a deep magma-poor margin based on seismic reflection data (northeastern Gulf of Aden margin, offshore Oman), *Geophys J Int*, *180*(2), 501-519.

Bai, Y., et al. (2015), Full-fit reconstruction of the South China Sea conjugate margins, *TECTONOPHYSICS*, *661*, 121-135.

Bai, Y., et al. (2019), Crustal stretching style variations in the northern margin of the South China Sea, *Tectonophysics*, *751*, 1-12, doi:https://doi.org/10.1016/j.tecto.2018.12.012.

Barckhausen, U., et al. (2014), Evolution of the South China Sea: Revised ages for breakup and seafloor spreading, *MAR PETROL GEOL*, *58*, 599-611.

Beranek, L. P. (2017), A magma-poor rift model for the Cordilleran margin of western North America, *GEOLOGY*, *45*(12), 1115-1118.

Boillot, G., et al. (1987), Tectonic denudation of the upper mantle along passive margins: a model based on drilling results (ODP leg 103, western Galicia margin, Spain), *TECTONOPHYSICS*, *132*(4), 335-342.

Briais, A., et al. (1993), Updated Interpretation of Magnetic Anomalies and Seafloor Spreading Stages in the South China Sea: Implications for the Tertiary Tectonics of Southeast Asia, *Journal of Geophysical Research*, *98*(B4), 6299-6328.

Brune, S., et al. (2017), Rifted margin architecture and crustal rheology: Reviewing Iberia-Newfoundland, Central South Atlantic, and South China Sea, *MAR PETROL GEOL*, *79*, 257-281.

Braun, J., and C. Beaumont (1989), A physical explanation of the relation between flank uplifts and the breakup unconformity at rifted continental margins, *Geology*, *17*(8), 760-764, doi:10.1130/0091-7613(1989)017<0760:APEOTR>2.3.CO;2.

Cameselle, A. L., et al. (2015), The continent‐ocean transition on the northwestern South China Sea, *Basin Res*, doi:doi: 10.1111/bre.12137.

Cao, L., et al. (2015), Provenance of Upper Miocene sediments in the Yinggehai and Qiongdongnan basins, northwestern South China Sea: Evidence from REE, heavy minerals and zircon U–Pb ages, *MAR GEOL*, *361*(0), 136-146.

Cao, L., et al. (2018), Early Miocene birth of modern Pearl River recorded low-relief, high elevation surface formation of SE Tibetan Plateau, *Earth Planet Sc Lett*, 496, 120-131, doi:https://doi.org/10.1016/j.epsl.2018.05.039.

Clift, P. D., et al. (2006), Thermochronology of mineral grains in the Red and Mekong Rivers, Vietnam: Provenance and exhumation implications for Southeast Asia, *Geochem Geophy Geosy*, *7*(10), doi:10.1029/2006GC001336.Compston, W., et al. (1992), Zircon U-Pb ages for the Early Cambrian time-scale, *J GEOL SOC LONDON*, *149*(2), 171-184.

Corti, G., et al. (2007), Tectonic inheritance and continental rift architecture: Numerical and analogue models of the East African Rift system, *Tectonics*, *26*(6), doi:10.1029/2006TC002086.

Cui, Y., et al. (2018), Upper Miocene–Pliocene provenance evolution of the Central Canyon in northwestern South China Sea, *Mar Geophys Res*, 1-13, doi:10.1007/s11001-018-9359-2.

Decarlis, A., et al. (2015), The tectono-stratigraphic evolution of distal, hyper-extended magma poor conjugate rifted margins: Examples from the Alpine Tethys and Newfoundland-Iberia, *Mar Petrol Geol*, *68*(A), 54-72, doi:10.1016/j.marpetgeo.2015.08.005.

Driscoll, N. W., and G. D. Karner (1999), Lower crustal extension across the Northern Carnarvon basin, Australia: Evidence for an eastward dipping detachment, *Journal of Geophysical Research*, *103*, 4975-4991.

Ding, W., et al. (2020), Lateral evolution of the rift-to-drift transition in the South China Sea: Evidence from multi-channel seismic data and IODP Expeditions 367&368 drilling results, *Earth Planet Sc Lett*, *531*, 115932, doi:https://doi.org/10.1016/j.epsl.2019.115932.

Ding, W., et al. (2018), Structures within the oceanic crust of the central South China Sea basin and their implications for oceanic accretionary processes, *Earth Planet Sc Lett*, *488*, 115-125, doi:https://doi.org/10.1016/j.epsl.2018.02.011.

Falvey (1974), The development of continental margins in plate tectonic theory, *J. Aust. Pet. Explor. Assoc.*, *14*, 95-106.

Franke, D., et al. (2014), The final rifting evolution in the South China Sea, *MAR PETROL GEOL*, *58*, 704-720.

Gao, J., et al. (2015), The continent–ocean transition 642 at the mid-northern margin of the South China Sea, Tectonophysics(654), 1-19.

Gao, J., et al. (2019), Post-seafloor spreading magmatism and associated magmatic hydrothermal systems in the Xisha uplift region, northwestern South China Sea, *Basin Res*, *31*(4), 688-708, doi:10.1111/bre.12338.

Gernigon, L., et al. (2012), The Norway Basin revisited: From continental breakup to spreading ridge extinction, *MAR PETROL GEOL*, *35*(1), 1-19.

Gillard, M., et al. (2015), Tectonomagmatic evolution of the final stages of rifting along the deep conjugate Australian-Antarctic magma-poor rifted margins: Constraints from seismic observations, *TECTONICS*, *34*(4), 753-783.

Hall, R. (2012), Late Jurassic–Cenozoic reconstructions of the Indonesian region and the Indian Ocean, *Tectonophysics*, *570-571*, 1-41, doi:https://doi.org/10.1016/j.tecto.2012.04.021.

Hart, B. S. (1999), Definition of subsurface stratigraphy, structure and rock properties from 3-D seismic data, *Earth-Sci Rev*, *47*(3–4), 189-218.

Haupert, I., et al. (2016), Upper-plate magma-poor rifted margins: Stratigraphic architecture and structural evolution, *Marine & Petroleum Geology*, *69*, 241-261.

He, Y., et al. (2011), Architecture and Characteristics of Mass Transport Deposits(MTDs) in Qiongdongnan Basin in Northern South China Sea, *Earth Science*, *36*(5), 905-913, doi:10.1130/B35001.1.

Hoang, L. V., et al. (2009), Evaluating the evolution of the Red River system based on in situ U-Pb dating and Hf isotope analysis of zircons, *Geochem. Geophys. Geosyst.*, 10(11), Q11008.

Holloway, N. H. (1982), North Palawan block, Philippines-its relation to Asian mainland and role in evolution of South China Sea, *American Association of Petroleum Geologists Bulletin*, *66*(9), 1355-1383.

Huang, H., et al. (2017), Condensate origin and hydrocarbon accumulation mechanism of the deepwater giant gas field in western South China Sea:A case study of Lingshui 17-2 gas field in Qiongdongnan Basin,South China Sea, *Petroleum Exploration & Development*, *44*(3), 409-417.

Huismans, R. S., and C. Beaumont, 2007, Roles of lithospheric strain softening and heterogeneity in determining the geometry of rifts and continental margins, *in* G. D. Karner, G. Manatschal, and L. M. Pinheiro, eds., Imaging, Mapping and Modelling Continental Lithosphere Extension and Breakup., v. 282, p. 111-138.

Huismans, R., and C. Beaumont (2011), Depth-dependent extension, two-stage breakup and cratonic underplating at rifted margins, *NATURE*, *473*(7345), 74-78.

Hunt, J. M. (1996), *Petroleum geochemistry and geology*, W.H Freeman and Company, New Youk.

Jian, Z., et al. (2019), Discovery of the marine Eocene in the northern South China Sea, *Natl Sci Rev*, *6*(5), 881-885, doi:10.1093/nsr/nwz084.

Jonell, T. N., et al. (2016), Controls on erosion patterns and sediment transport in a monsoonal, tectonically quiescent drainage, Song Gianh, Central Vietnam, *Basin Res*, *29*(S1), 659-683, doi:10.1111/bre.12199.

Larsen, H. C., et al. (2018), Rapid transition from continental breakup to igneous oceanic crust in the South China Sea, *NAT GEOSCI, 11*(10), 782-789, doi:10.1038/s41561-018-0198-1..

Lei, C., and J. Ren (2016), Hyper-extended rift systems in the Xisha Trough: implications for extreme crustal thinning ahead of a propagating ocean of the South China Sea, *MAR PETROL GEOL*, *77*, 846-864.

Lei, C., et al. (2018), Continental rifting and sediment infill in the distal part of the northern South China Sea in the Western Pacific region: Challenge on the present-day models for the passive margins, *MAR PETROL GEOL*, *93*, 166-181.

Lei, C., et al. (2019a), Depositional architecture and structural evolution of a region immediately inboard of the locus of continental breakup (Liwan Sub-basin, South China Sea), *Geol Soc Am Bull*, *131*(7-8), 1059-1074, doi:10.1130/B35001.1.

Lei, C., et al. (2019b), A rapid shift in the sediment routing system of lower-upper Oligocene strata in the qiongdongnnan basin (Xisha Trough), Northwest south China Sea, *Mar Petrol Geol*, 104, 249-258, doi:https://doi.org/10.1016/j.marpetgeo.2019.03.012.

Li, C., et al. (2014), Ages and magnetic structures of the South China Sea constrained by deep tow magnetic surveys and IODP Expedition 349, *Geochemistry, Geophysics, Geosystems*, *15*, 4958-4983.

Li, C., et al. (2015), Seismic stratigraphy of the central South China Sea basin and implications for neotectonics, *Journal of Geophysical Research: Solid Earth*, *120*(3), 1377-1399.

Li, L., et al. (2014), Non-uniform hyper-extension in advance of seafloor spreading on the vietnam continental margin and the SW South China Sea, *BASIN RES*, *26*(1), 106-134.

Lizarralde, D. et al. (2007), Variation in styles of rifting in the Gulf of California, *Nature* 448:466–469.

Lymer, G., et al. (2019), 3D development of detachment faulting during continental breakup, *Earth Planet Sc Lett*, *515*, 90-99, doi:https://doi.org/10.1016/j.epsl.2019.03.018.

Manatschal, G. (2004), New models for evolution of magma-poor rifted margins based on a review of data and concepts from West Iberia and the Alps, *INT J EARTH SCI*, *93*(3), 432-466.

Marfurt, K. J., and T. M. Alves (2014), Pitfalls and limitations in seismic attribute interpretation of tectonic features, *Interpretation*, *3*(1), B5-B15, doi:10.1190/INT-2014-0122.1.

Masini, E., et al. (2012), Anatomy and tectono-sedimentary evolution of a rift-related detachment system: The example of the Err detachment (central Alps, SE Switzerland), *GEOL SOC AM BULL*, *124*(9-10), 1535-1551.

Masini, E., et al. (2013), The Alpine Tethys rifted margins: Reconciling old and new ideas to understand the stratigraphic architecture of magma‐poor rifted margins, *Sedimentology*, *60*(1), 174-196.

McIntosh, K., et al. (2014), Crustal structure and inferred rifting processes in the northeast South China Sea, *MAR PETROL GEOL*, *58*(B), 612-626.

McKenzie, D. (1978), Some remarks on the development of sedimentary basins, *EARTH PLANET SC LETT*, *40*(1), 25-32.

Mohn, G., et al. (2012), Necking of continental crust in magma-poor rifted margins: Evidence from the fossil Alpine Tethys margins, *TECTONICS*, *31*(1), doi:10.1029/2011TC002961.

Morley, C. K. (2016), Major unconformities/termination of extension events and associated surfaces in the South China Seas: Review

and implications for tectonic development, *J ASIAN EARTH SCI*, *120*, 62-86.

Nemčok, M., et al. (2013), East Indian margin evolution and crustal architecture: integration of deep reflection seismic interpretation and gravity modelling, *Geological Society, London, Special Publications*, *369*(1), 477-496.

Pereira, R., and T. M. Alves (2012), Tectono-stratigraphic signature of multiphased rifting on divergent margins (deep-offshore southwest Iberia, North Atlantic), *Tectonics*, *31*(TC4001), doi:10.1029/2011TC003001.

Peron-Pinvidic, G., and G. Manatschal (2009), The final rifting evolution at deep magma-poor passive margins from Iberia-Newfoundland: a new point of view, *INT J EARTH SCI*, *98*(7), 1581-1597.

Peron-Pinvidic, G., and P. T. Osmundsen (2016), Architecture of the distal and outer domains of the Mid-Norwegian rifted margin: Insights from the Rån-Gjallar ridges system, *MAR PETROL GEOL*, *77*, 280-299.

Peron-Pinvidic, G., et al. (2013), Structural comparison of archetypal Atlantic rifted margins: a review of observations and concepts, *MAR PETROL GEOL*, *43*, 21-47.

Qiu, X., et al. (2001), Crustal structure across the Xisha trough, northwestern South China Sea, *Tectonophysics*, *341*(1-4), 179-193.

Ranero, C. R., and M. Perez-Gussinye (2010), Sequential faulting explains the asymmetry and extension discrepancy of conjugate margins, *NATURE*, *468*(7321), 294-299.

Reston, T. J. (2009), The structure, evolution and symmetry of the magma-poor rifted margins of the North and Central Atlantic: A synthesis, *TECTONOPHYSICS*, *468*(1-4), 6-27.

Ru, K., and J. D. Pigott (1986), Episodic rifting and subsidence in the South China Sea, *AAPG BULL*, *70*(9), 1136-1155.

Savva, D., et al. (2013), Seismic evidence of hyper-stretched crust and mantle exhumation offshore Vietnam, *TECTONOPHYSICS*, *608*, 72-83.

Savva, D., et al. (2014), Different expressions of rifting on the South China Sea margins, *Mar Petrol Geol*, *58, Part B*(0), 579-598, doi:http://dx.doi.org/10.1016/j.marpetgeo.2014.05.023.

Sawyer, D. S., R. B. Whitmarsh, A. Klaus, and E. Al., 1994, Proceedings of the ODP. Initial Reports, 149. Ocean Drilling Program, College Station, TX.

Searle, R., 2013, Mid-Ocean Ridges, Cambridge University Press, UK. https://doi.org/10.1017/CBO9781139084260

Shao, L., et al. (2016), Detrital zircon provenance of the Paleogene syn‐rift sediments in the northern South China Sea, *Geochemistry, Geophysics, Geosystems*, 17(2), 255-269.

Shao, L., et al. (2017a), Detrital zircon ages and elemental characteristics of the Eocene sequence in IODP Hole U1435A: Implications for rifting and environmental changes before the opening of the South China Sea, *Mar Geol*, 394, 39-51, doi:https://doi.org/10.1016/j.margeo.2017.08.002.

Shao, L., et al. (2017b), Cretaceous–Eocene provenance connections between the Palawan Continental Terrane and the northern South China Sea margin, *Earth Planet Sc Lett*, 477, 97-107, doi:https://doi.org/10.1016/j.epsl.2017.08.019.

Shao, L., et al. (2019), Drainage control of Eocene to Miocene sedimentary records in the southeastern margin of Eurasian Plate, *Geol Soc Am Bull*, 131(3-4), 461-478, doi:10.1130/B32053.1.

Sibuet, J., and B. E. Tucholke (2013), The geodynamic province of transitional lithosphere adjacent to magma-poor continental margins, *Geological Society, London, Special Publications*, *369*(1), 429-452.

Sibuet, J., et al. (2016), Geodynamics of the South China Sea, *TECTONOPHYSICS*, *692*(B), 98-119.

Soares, D. M., et al. (2012), The breakup sequence and associated lithospheric breakup surface:Their significance in the context of rifted continental margins (West Iberia and Newfoundland margins, North Atlantic), *Earth Planet Sc Lett*, *355-356*, 311-326, doi:10.1016/j.epsl.2012.08.036.

Su, M., et al. (2019), Late Miocene provenance evolution at the head of Central Canyon in the Qiongdongnan Basin, Northern South China Sea, *Mar Petrol Geol*, *110*, 787-796, doi:https://doi.org/10.1016/j.marpetgeo.2019.07.053.

Sun, W., et al. (2009), Detrital zircon U–Pb geochronological and Lu–Hf isotopic constraints on the Precambrian magmatic and crustal evolution of the western Yangtze Block, SW China, *Precambrian Res*, 172(1), 99-126.

Taylor, B., and D. E. Hayes (1983), Origin and History of the South China Sea Basin, in *The Tectonic and Geologic Evolution of Southeast Asian Seas and Islands (Part 2)*, edited by D. E. Hayes, pp. 23-56, American Geophysical Union Geophysical Monograph Series.

Tucholke, B. E., D. S. Sawyer, and J. C. Sibuet, 2007, Breakup of the Newfoundland-Iberia rift: Geological Society of London Special Publications, v. 282, p. 9-46.

Tugend, J., et al. (2014), Characterizing and identifying structural domains at rifted continental margins: application to the Bay of Biscay margins and its Western Pyrenean fossil remnants, *Geological Society, London, Special Publications*, *413*, P413.

Unternehr, P., et al. (2010), Hyper-extended crust in the South Atlantic: in search of a model, *PETROL GEOSCI*, *16*(3), 207-215.

Vermeesch, P. (2004), How many grains are needed for a provenance study? *Earth and Planerary Science Letters*, *224*(3-4), 441-451.

Wang, C., et al. (2015), Detrital zircon record of sediments from six modern rivers: geochronology and its implications, Western Hainan, China, *Earth Science Frontiers*, 22(4), 277-289.

Wang, C., et al. (2018), Linking source and sink: Detrital zircon provenance record of drainage systems in Vietnam and the Yinggehai−Song Hong Basin, South China Sea, *GSA Bulletin*, 131(1-2), 191-204.

Wang, J., et al. (2018), The Baiyun and Liwan Sags: Two supradetachment basins on the passive continental margin of the northern South China Sea, *Mar Petrol Geol*, *95*, 206-218, doi:https://doi.org/10.1016/j.marpetgeo.2018.05.001.

Wang, P., W. L. Prell, P. Blum, and S. S. Party, 2000, Proceedings of Ocean Drilling Program, Initial Report, Vol. 184, College Station, Tex., Ocean Drill. Program.

Wang, Z., et al. (2014), Vertical migration through faults and hydrocarbon accumulation patterns in deepwater areas of the Qiongdongnan Basin, *ACTA OCEANOL SIN*, *33*(12), 96-106.

Wernicke, B. (1981), Low-angle normal faults in the Basin and Range Province: nappe tectonics in an extending orogen, *Nature*, *291*, 645-648.

Wernicke, B. (1985), Uniform-sense normal simple shear of the continental lithosphere, *CAN J EARTH SCI*, *22*(1), 108-125.

Whitmarsh, R. B., M. O. Beslier, P. J. Wallace, and Etal, 1997, Proceedings of the Ocean Drilling Program. Initial Reports, vol. 173. Ocean Drill. Program, College Station, Tex.

Wu, J., et al. (2016), Philippine Sea and East Asian plate tectonics since 52 Ma constrained by new subducted slab reconstruction methods, *Journal of Geophysical Research: Solid Earth*, *121*(6), 4670-4741, doi:10.1002/2016JB012923.

Xia, S., et al. (2010), Crustal structure in an onshore-offshore transitional zone near Hong Kong, northern South China Sea, *J ASIAN EARTH SCI*, *37*(5-6), 460-472.

Xia, Y., et al. (2012), Paleoproterozoic S- and A-type granites in southwestern Zhejiang: Magmatism, metamorphism and implications for the crustal evolution of the Cathaysia basement, *PRECAMBRIAN RES*, *216–219*, 177-207.

Xie, Y., et al. (2015), *The theory and practice of high temperature overpressure gas accumulation in the Yinggehai and Qiongdongnan Basins*, Petroleum Industry Press, Beijing (In Chinese with English Abstract).

Xu, Y., et al. (2008), Zircon U–Pb and Hf isotope constraints on crustal melting associated with the Emeishan mantle plume, *Geochim Cosmochim Ac*, 72(13), 3084-3104.

Xu, Y., et al. (2014), The U–Pb ages and Hf isotopes of detrital zircons from Hainan Island, South China: implications for sediment

provenance and the crustal evolution, *Environ Earth Sci*, 71(4), 1619-1628.

Yan, Y., et al. (2011), Understanding sedimentation in the Song Hong-Yinggehai Basin, South China Sea, *Geochem. Geophys. Geosyst*., 12(6), Q6014.

Yao, J., et al. (2011), Detrital zircon U–Pb geochronology, Hf-isotopes and geochemistry—New clues for the Precambrian crustal evolution of Cathaysia Block, South China, *Gondwana Res*, 20(2–3), 553-567, doi:https://doi.org/10.1016/j.gr.2011.01.005.

Yeh, Y., et al. (2012), Crustal features of the northeastern South China Sea: insights from seismic and magnetic interpretations, *MAR GEOPHYS RES*, 33(4), 307-326, doi:10.1007/s11001-012-9154-4.

Yuan, Y., et al. (2009), "Uniform geothermal gradient" and heat flow in the Qiongdongnan and Pearl River Mouth Basins of the South China Sea, *MAR PETROL GEOL*, *26*(7), 1152-1162.

Zhang, L., and S. Chen (2017), Reservoir property response relationship under different geothermal gradients in the eastern area of the Pearl River Mouth basin, *China Offshore Oil and Gas*, *29*(1), 29-38.

Zhao, F., et al. (2016), Prolonged post-rift magmatism on highly extended crust of divergent continental margins (Baiyun Sag, South China Sea), *Earth and Planetary Science Letters*, *445*, 79-91.

Zhao, Y., et al. (2018a), Structural style, formation of low angle normal fault and its controls on the evolution of Baiyun Rift, northern margin of the South China Sea, *MAR PETROL GEOL*, *89*, 687-700.

Zhao, Z., et al. (2018b), Cenozoic tectonic subsidence in the Qiongdongnan Basin, northern South China Sea, *Basin Res*, *30*(S1), 269-288, doi:10.1111/bre.12220.

Zhao, Z., et al. (2015), The high resolution sedimentary filling in Qiongdongnan Basin, Northern South China Sea, *MAR GEOL*, *361*(0), 11-24.

Zhao, M., et al. (2019), Intermingled fates of the South China Sea and Philippine Sea plate, *Natl Sci Rev* , *6*(5), 886-890, doi:10.1093/nsr/nwz107.

Zhu, W., et al. (2017), New insights on the origin of the basement of the Xisha Uplift, South China Sea, *Science China Earth Sciences*, 60(12), 2214-2222, doi:10.1007/s11430-017-9089-9.

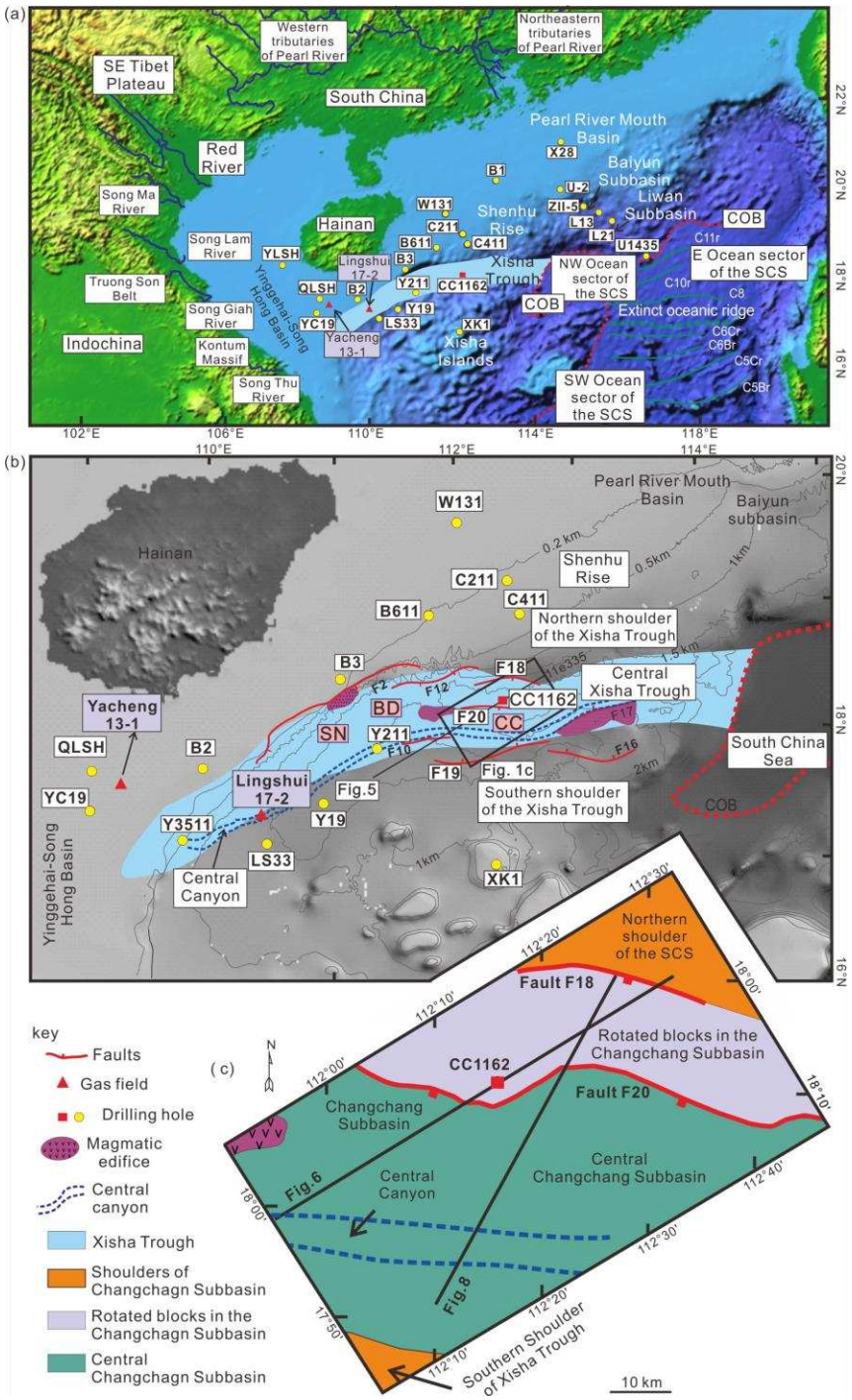

Figure 1 (a) Map of the northern South China Sea showing the relative location of the Xisha Trough. The location of gas fields is based on *Wang et al.* [2014] and *Huang et al.* [2017]. The dashed red line highlights the position of the continent-ocean boundary (COB). (b) Bathymetric map of the Xisha Trough showing the full coverage of 3D seismic data used in this work, i.e., in the deepwater region just landward of the oceanic ridge of the South China Sea. SN: Songnan Subbasin; BD: Baodao Subbasin; CC: Changchang Subbasin. (c) Main structural units in the area of the interpreted 3D seismic volume (CVX3D). The figure shows the location of Exploration Well CC1162 and interpreted seismic profiles.

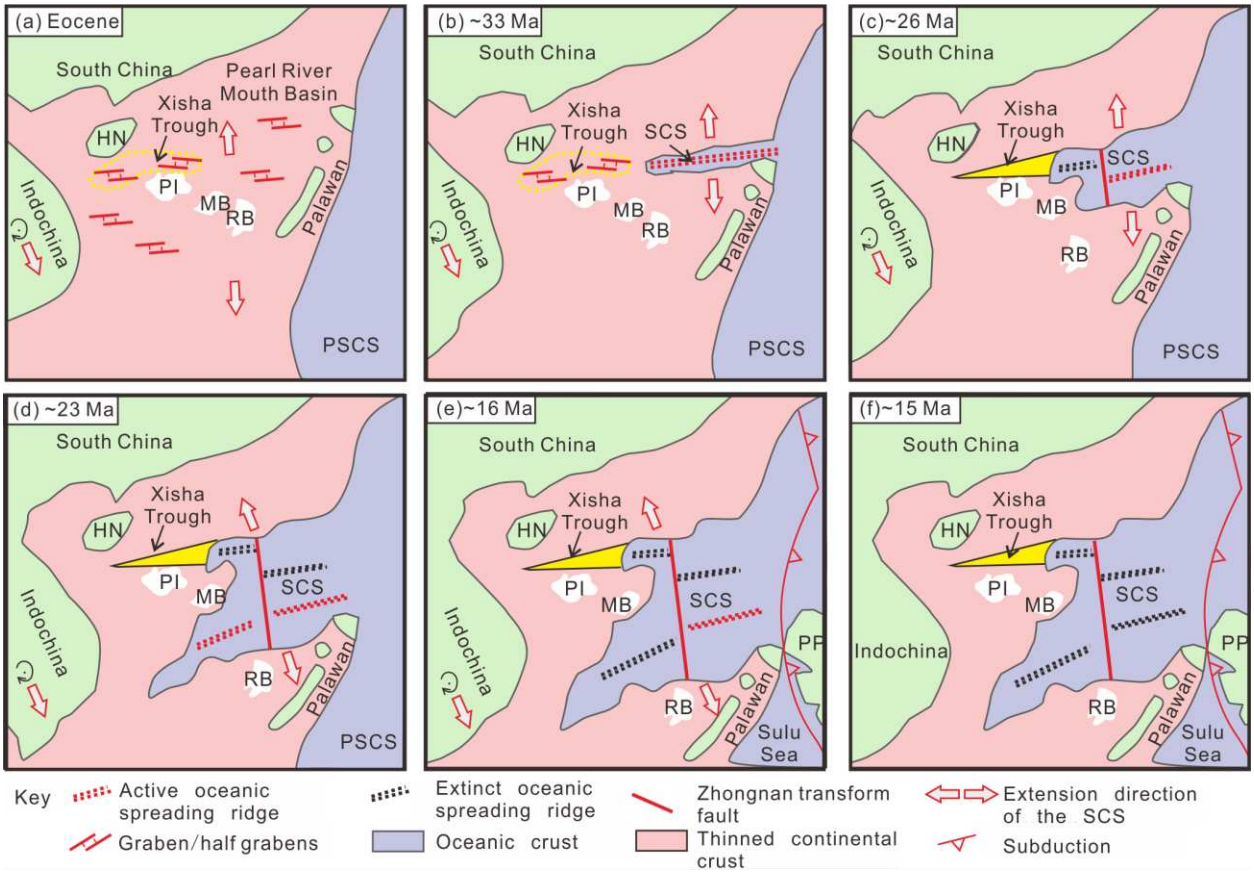

Figure 2 Schematic representation of progressive continental breakup in the SCS. (a) Widespread continental rifting in the northern SCS; (b) Continental breakup and oceanic spreading in the Northwest Ocean Sector of the SCS; (c) Cessation of oceanic spreading in the Northwest Ocean Sector; (d) Oceanic spreading in the Southwest Ocean Sector; (e) Cessation of oceanic spreading in the Southwest Ocean Sector; (f) Post-spreading oceanic crust in the SCS. HN: Hainan Island; PI: Xisha Islands; MB: Macclesfield Bank; RB: Reed Bank; SCS: South China Sea. Modified from *Briais et al* [1993], *Sibuet et al*. [2016], *Li et al* [2014; 2015], *Wu et al* [2016], *Cameselle et al* [2015], *Zhao et al* [2019] and *Hall* [2012].

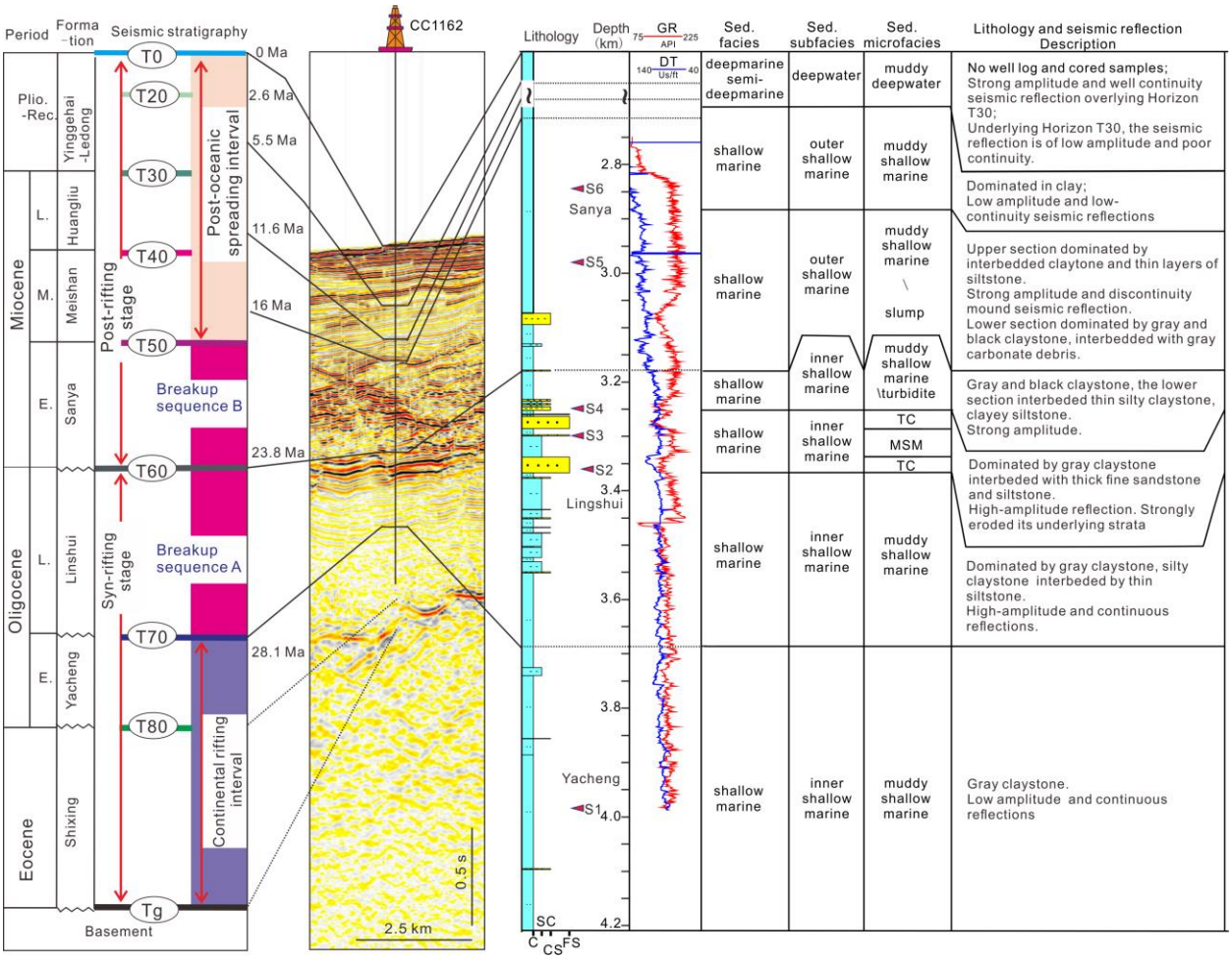

Figure 3 Stratigraphy of Cenozoic strata in the Xisha Trough, their ages and representative lithologies encountered by Exploration Well CC1162. Main stratigraphic units drilled by Well CC1162, described in the Figure, are correlated with key regional seismic-stratigraphic markers. C: claystone/clay; SC: silty claystone; CS: clayey siltstone; FS: fine sandstone; MSM: Muddy shallow marine; TC: Turbidite Channel.

S1
(depth: 3995m; Yacheng Formation)
dark gray mudstone

S2
(depth: 3368m; Lingshui Formation)
gray fine sandstone

S3
(depth: 3297m; Lingshui Formation)
gray fine sandstone

S4
(depth: 3246m; Lingshui Formation)
black gray siltstone

S5
(depth: 2970m; Sanya Formation)
gray calcareous claystone

S6
(depth: 2848m; Sanya Formation)
gray claystone

Figure 4 Photographs of rock samples S1, S2, S3, S4, S5 and S6 taken from Oligocene and Miocene strata drilled by Well CC1162. The relative depths at which these samples were collected are shown in Figure 3.

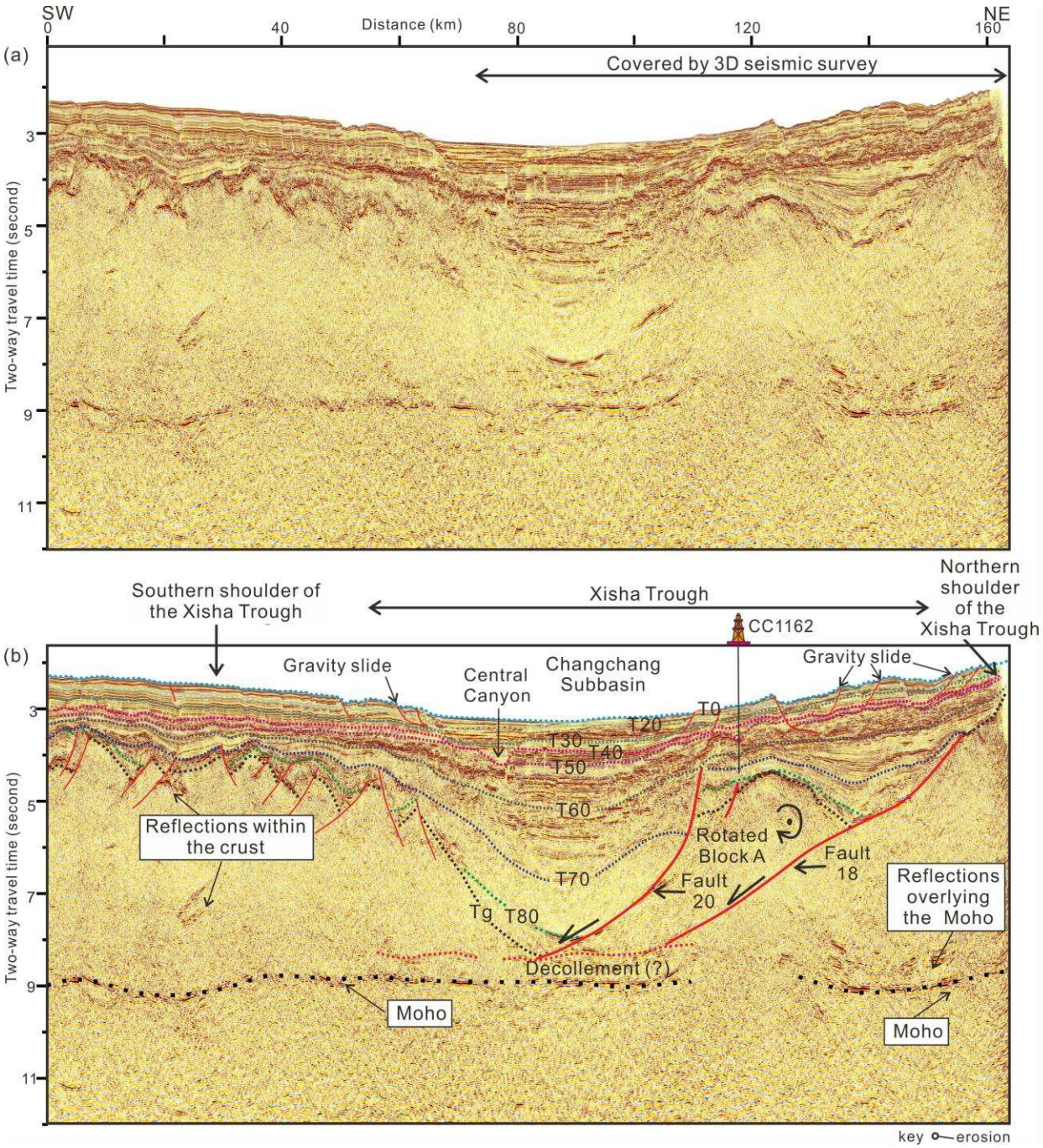

Figure 5 (a) Uninterpreted 2D seismic profile and (b) corresponding interpretation profile across the Changchang Subbasin and its northern and southern shoulders. The figure shows a series of rotated blocks, from which Block A is the largest, bounded by large listric faults propagating from (and soling out in) the pre-rift basement. The location of the seismic profile is shown in Figure 1b. The strong amplitude seismic reflection within the crust were indicated by the boxes.

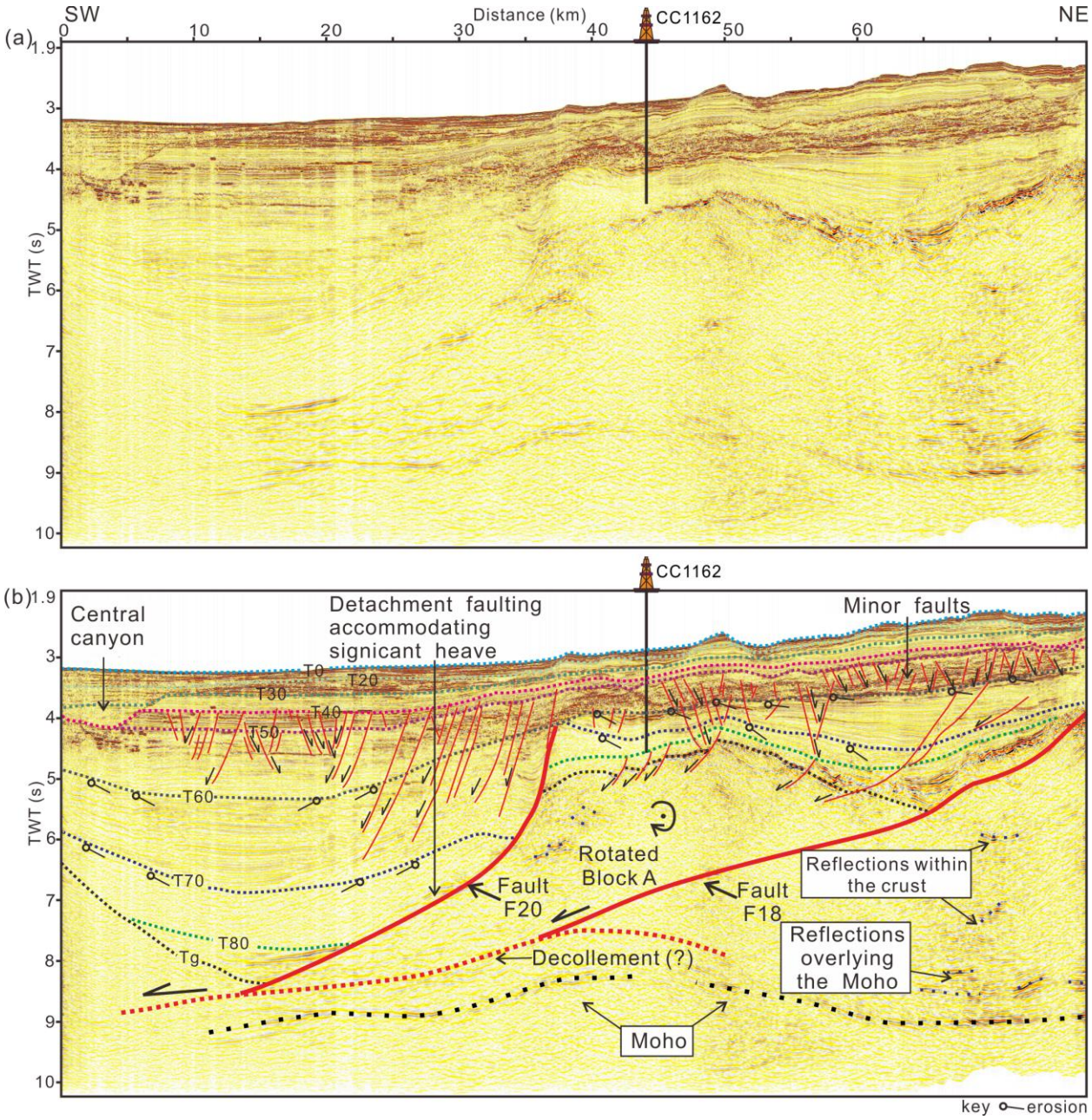

Figure 6 (a) Uninterpreted seismic profile and (b) corresponding interpretation showing the E-W-striking faults interpreted in the study area. The location of the seismic profile is shown in Figure 1c.

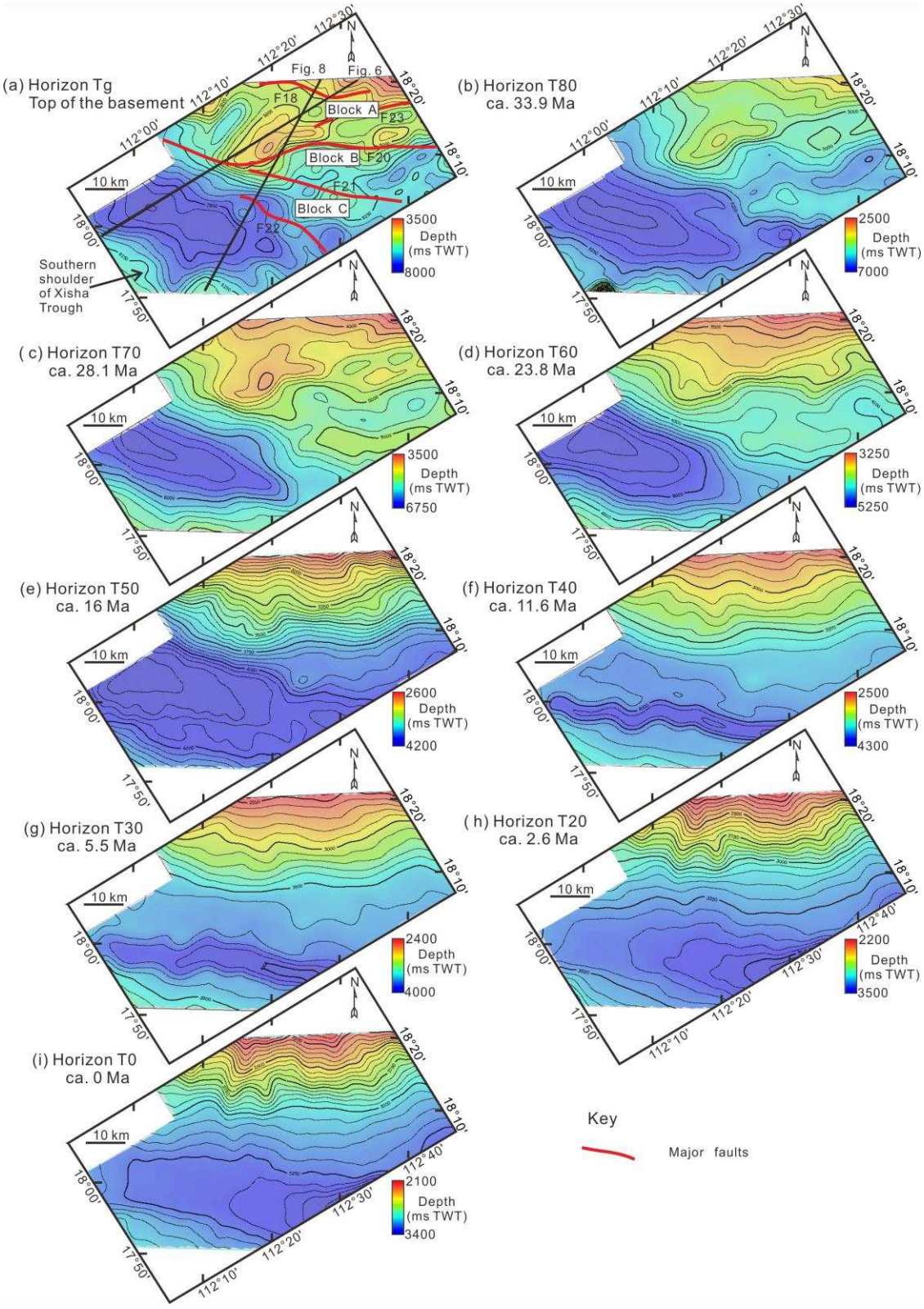

Figure 7 Two-way time (TWT) structural maps for main seismic-stratigraphic markers (Horizons Tg to T0) interpreted in the study area.

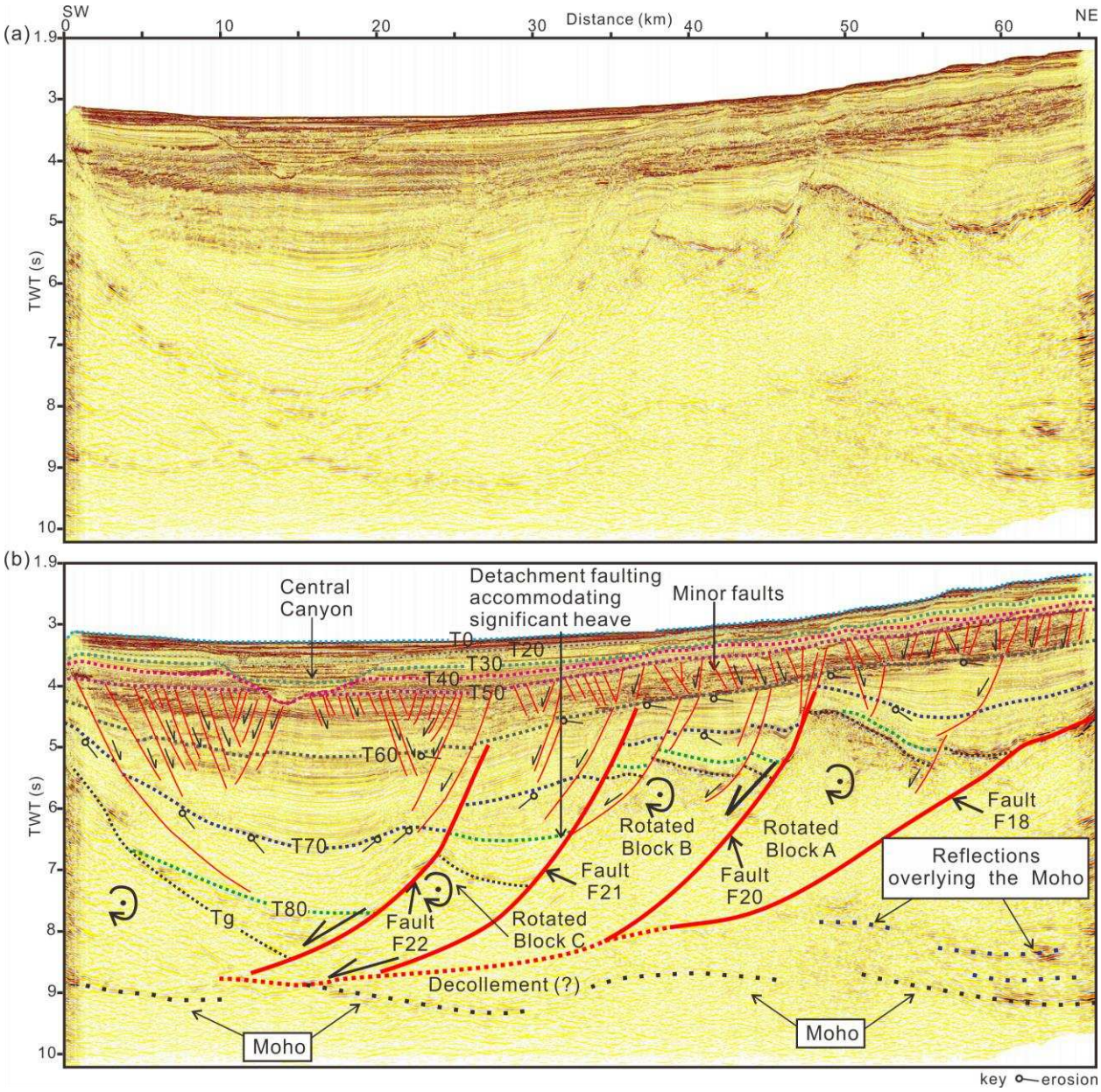

Figure 8 (a) Uninterpreted seismic profile and (b) corresponding interpretation section tied to Well CC1162. The location of the seismic profile is shown in Figure 1c.

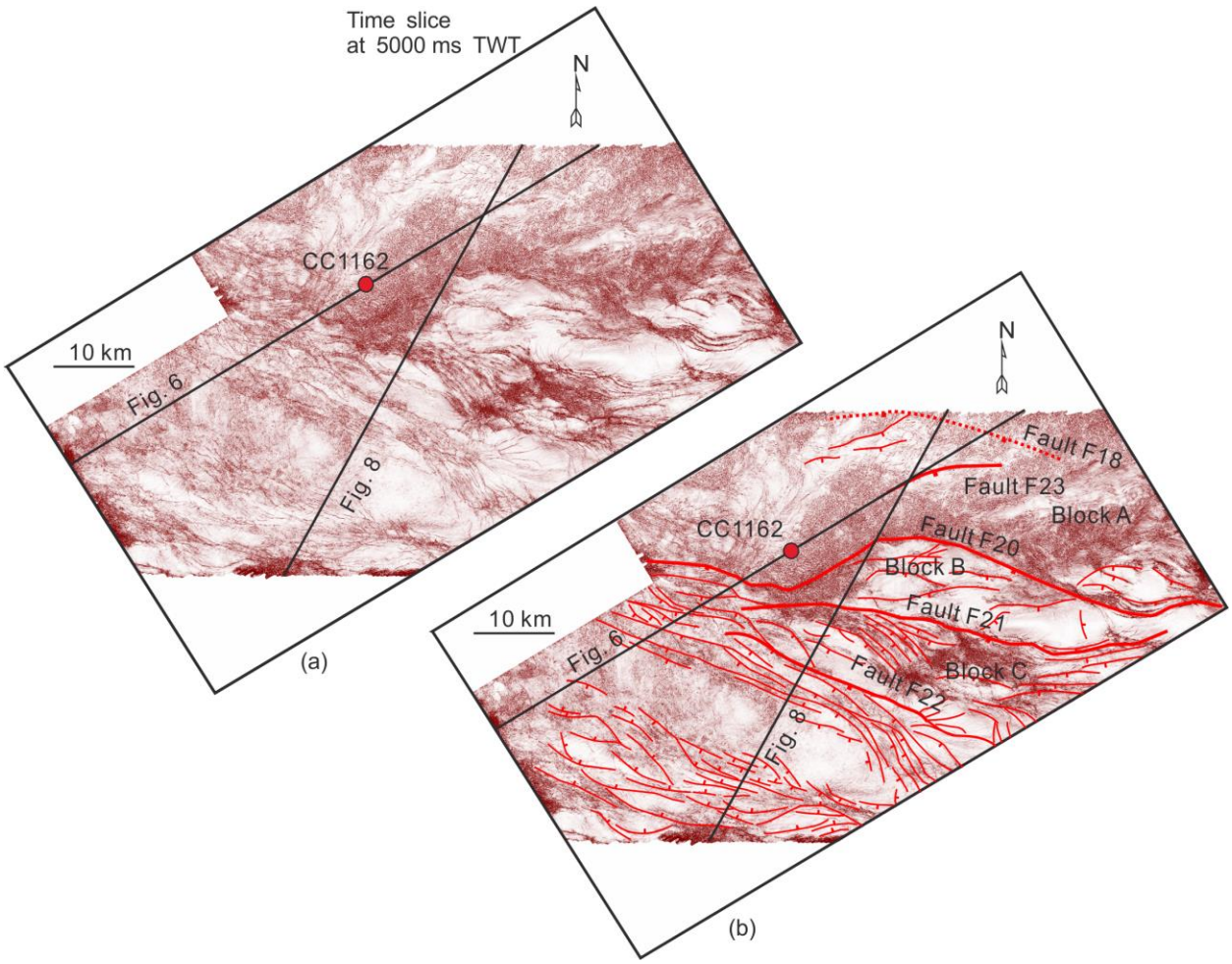

Figure 9 (a) Uninterpreted and (b) interpreted coherence time-slices at 5000 ms TWT, revealing a series of tectonic faults with a dominant E-W strike. Uniform seismic reflections in the northern part of the maps suggest the presence of basement rock at this structural level, hindering a better imaging of Fault F18 on coherence data. The dashed line highlights the strike of Fault F18 based on the interpretation of selected seismic profiles.

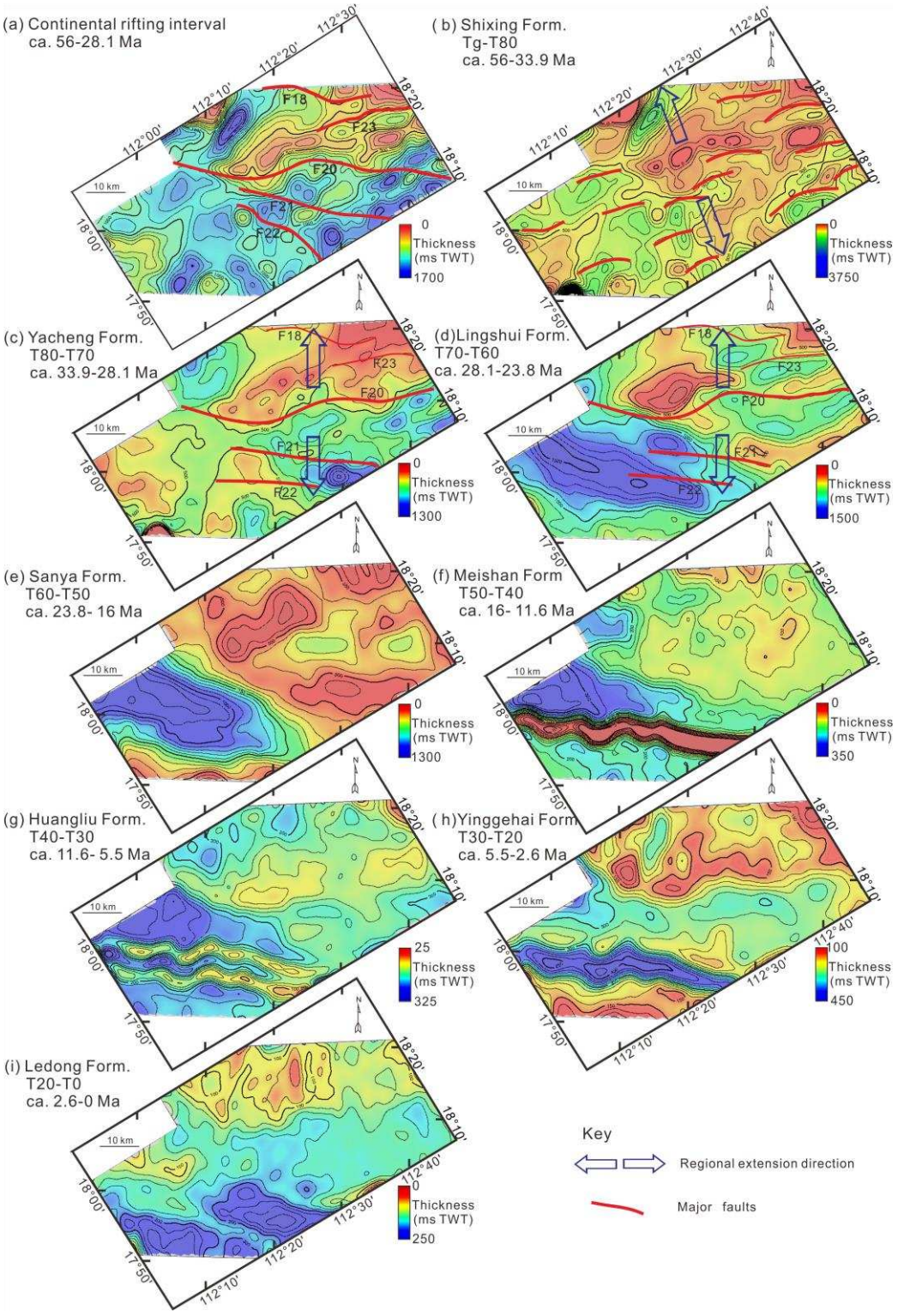

Figure 10 Isochron maps illustrating the thickness variations observed in key stratigraphic units filling the Changchang Subbasin. The maps summarize the temporal and spatial development of key structures in the subbasin. The faults shown in Figure 10(a) are after the result from coherence time-slice at 5000 ms TWT in Figure 9. The faults in Figures 10(b)-10(d) at different periods were interpreted from seismic profiles from 3D seismic survey.

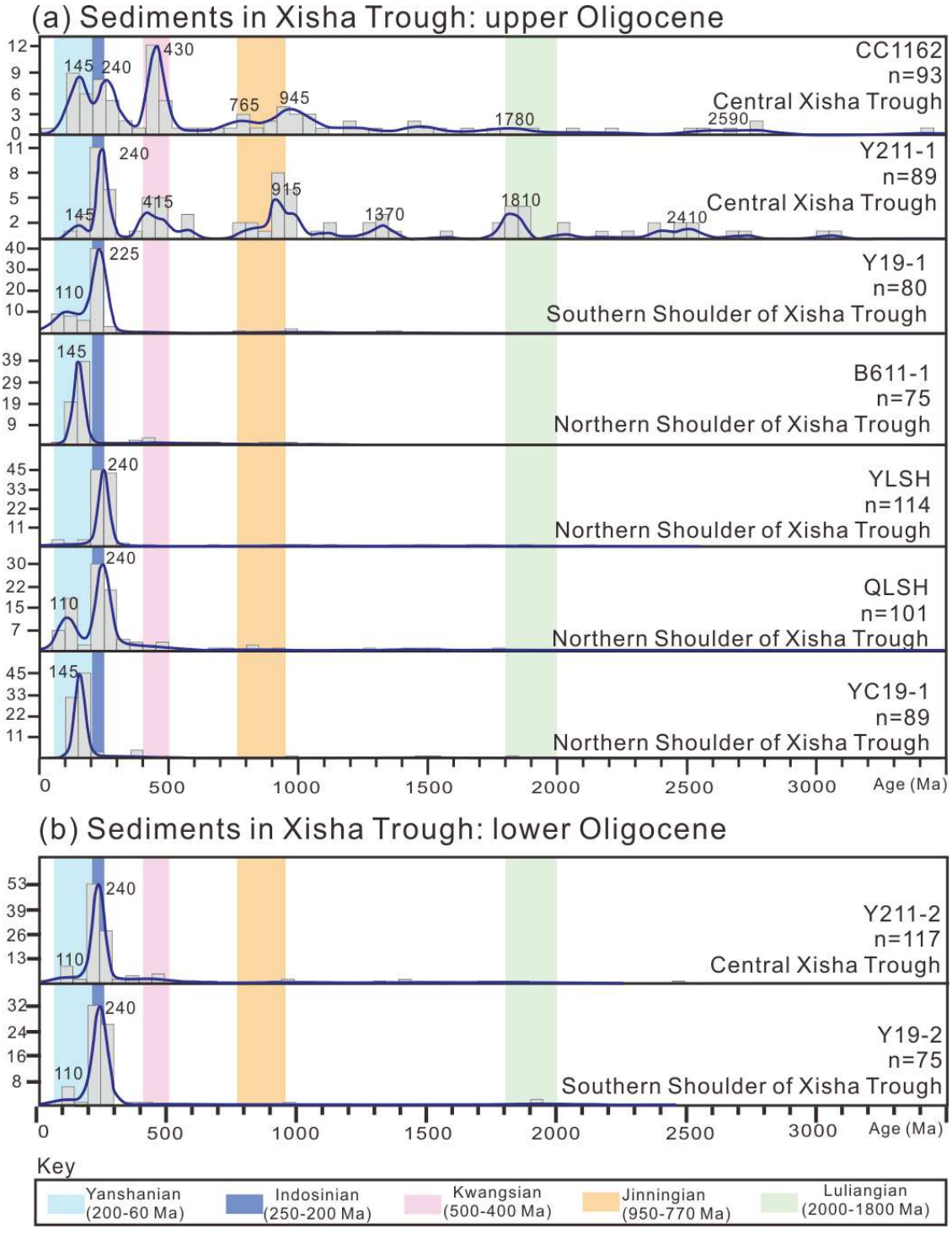

Figure 11 Kernel density estimate plots of analyzed U-Pb detrital zircon ages for upper Oligocene sediment in Well CC1126. U-Pb ages are compared to other Oligocene sediments in the Xisha Trough. The probability density diagrams were correlated with major regional tectonic events (colored bands). Note that the y-axis has no vertical scale. See Supplementary Table S1 for all compiled U-Pb age data.

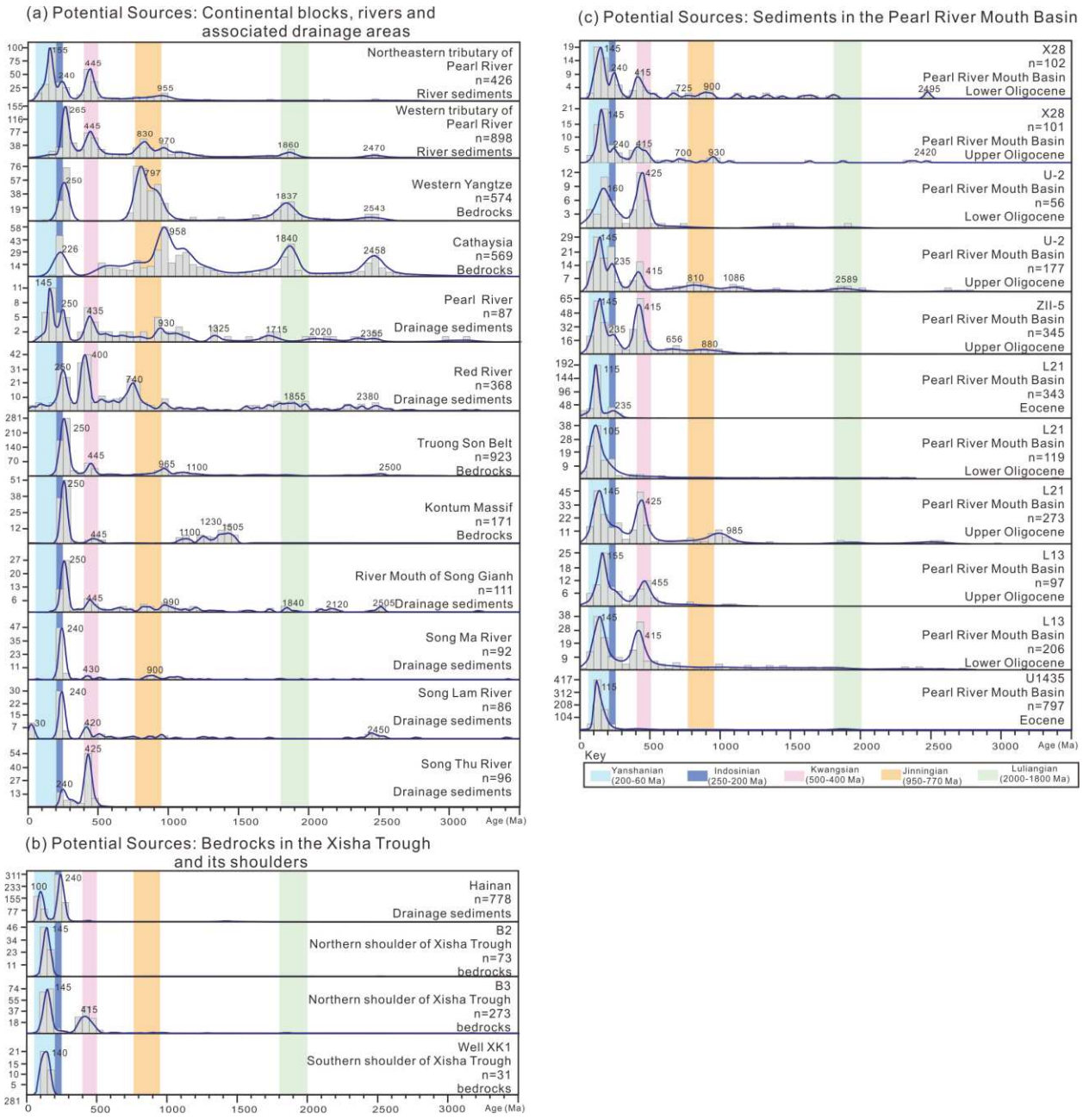

Figure 12 Kernel density estimate plots of analyzed U-Pb detrital zircon ages for potential sources of Oligocene sediment. See Supplementary Table S1 for all U-Pb age data acquired.

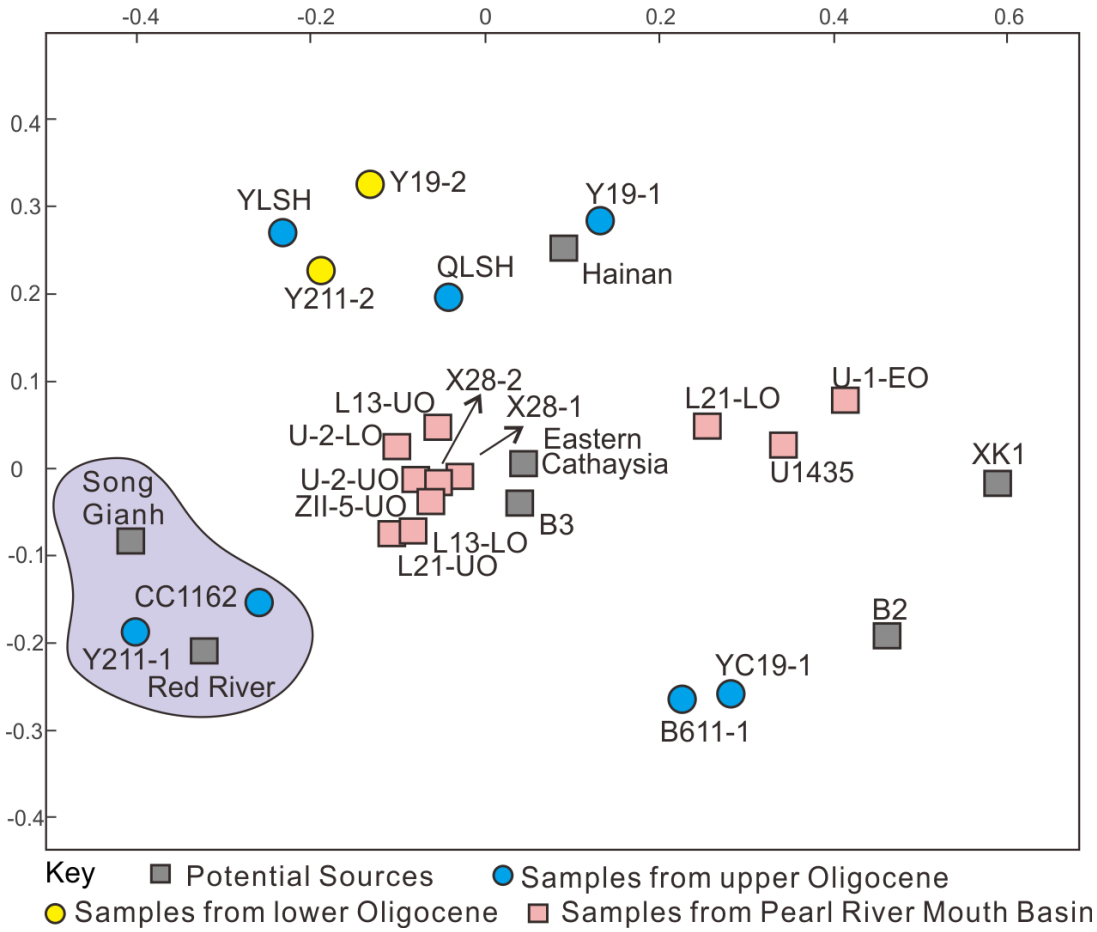

Figure 13 Non-metric multi-dimensional scaling (MDS) plot showing the similarities between samples of Oligocene sediment in the Xisha Trough and its potential sediment sources. The stress value of the MDS statistics is 0.097, indicating a fair goodness of fit [*Vermeesch, 2013*]. The closest samples are on the MDS plot, the more similar are their age spectra, e.g. samples from Upper Oligocene at sites of Exploration Wells CC1162, Y211, and river sands from modern Red and Song Gianh River (Violet colors).

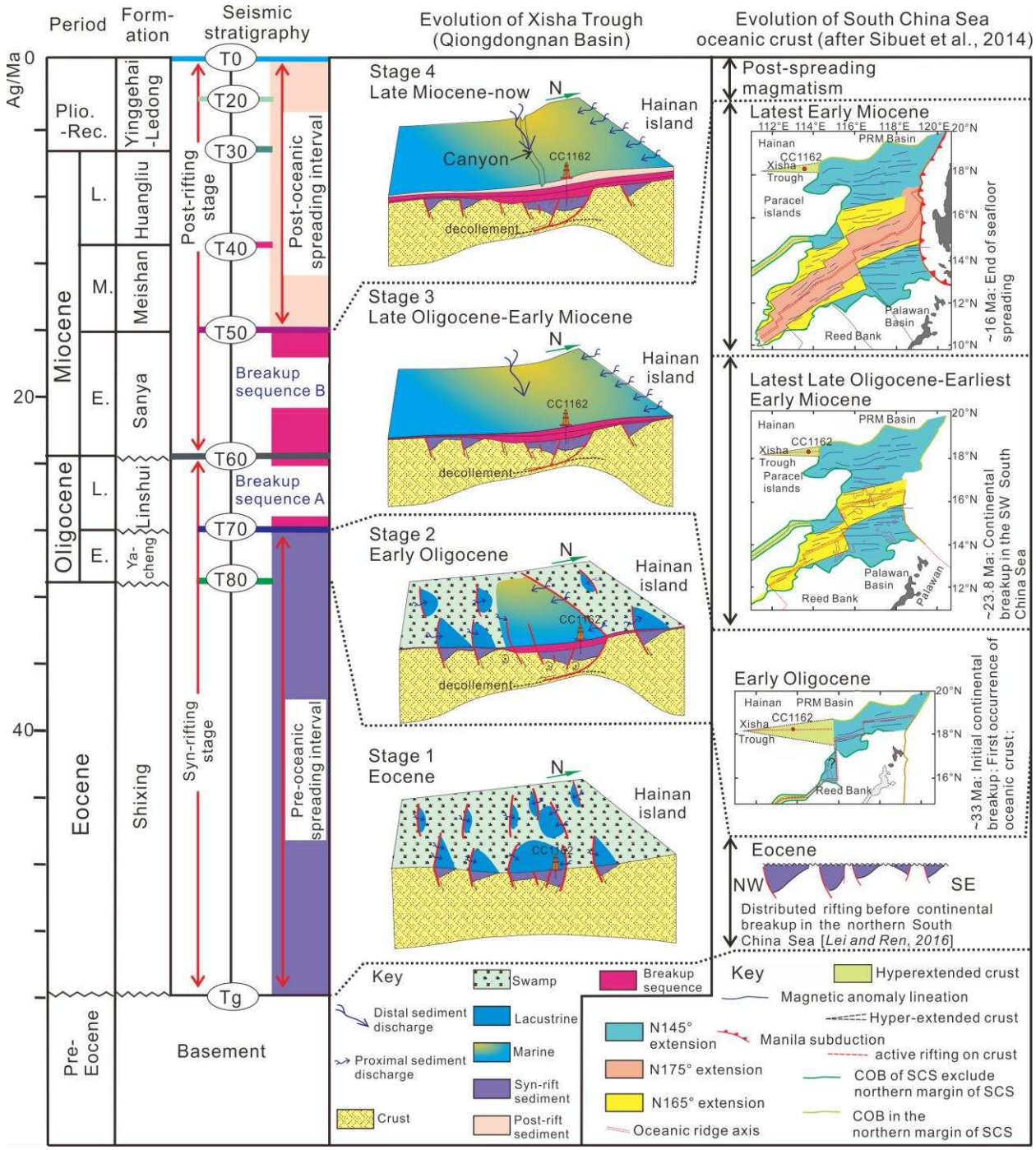

Figure 14 Schematic diagrams summarizing the tectono-sedimentary evolution of the Xisha Trough.